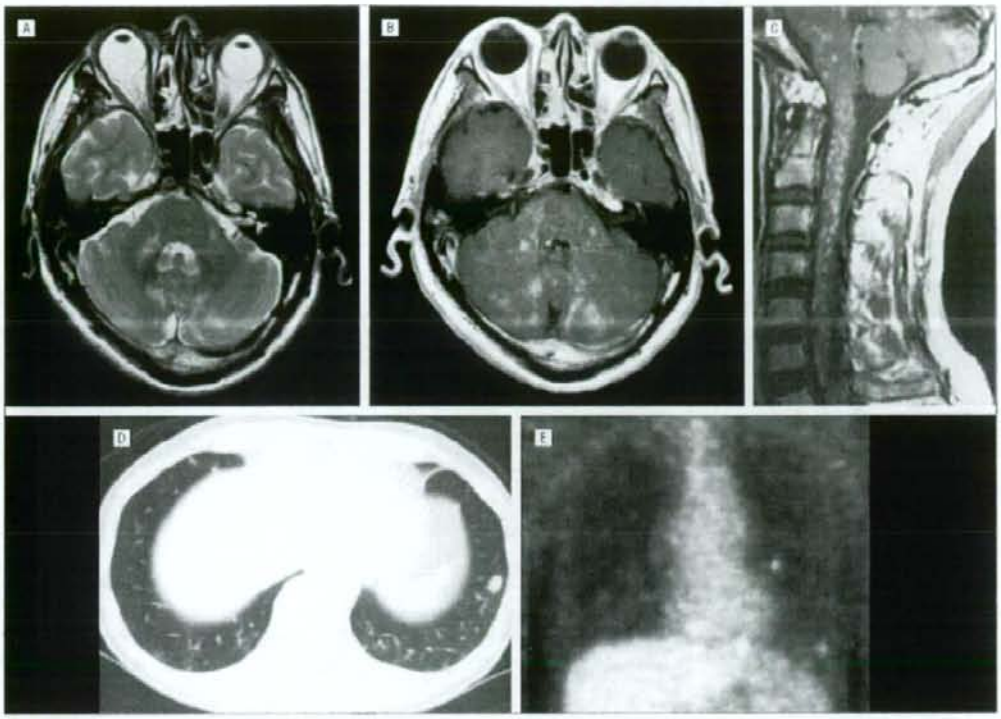

Figure 1. Magnetic resonance images of the head and spinal cord, computed tomographic scans of the lung, and [^{18}F]-fluorodeoxyglucose positron emission tomography (FDG-PET) of the body before treatment. A, Numerous spotty high-intensity lesions are observed in the pons and cerebellum on a T2-weighted image. B, These lesions are enhanced with gadolinium on a T1-weighted image. The lesions are also observed in the cerebral cortex to a lesser extent. C, A T1-weighted image with gadolinium enhancement of the cervical cord also demonstrates similar lesions. D and E, Nodular lesions are observed in the left lower lung and these lesions show abnormal FDG uptake, for which the maximum standard uptake value is 3.2.

continence. His gait worsened and he started to need a cane.

On admission to our hospital, his physical examination results were unremarkable except for atopic dermatitis. Neurological examination revealed spastic paraparesis with increased tendon reflexes in all his extremities and positive finger flexor reflexes. His plantar reflexes were extensor. He also had distal dominant dysesthesia of his lower limbs, spastic-type neurogenic bladder, and fecal incontinence. He was not able to run or go up the stairs. He could only walk with a cane for a short distance.

His serum soluble IL-2 receptor level was 550 U/ml (reference range, 167-497 U/ml). Anti–human immunodeficiency virus antibodies were not detected. His other laboratory results were unremarkable. His cerebrospinal fluid showed an elevated protein level (0.097 g/dl [to convert to grams per liter, multiply by 10]) and lymphocytic pleocytosis (28 cells/μl). The cytologic analysis showed no malignant cells. The test results for bacteria, *Mycobacterium tuberculosis*, and fungi were negative.

His nerve conduction study results, auditory brain stem response, and visually evoked potentials were normal. Short latency sensory evoked potentials of the right tibial nerve revealed slight elongation of central conduction time (19.6 milliseconds), but those of the left tibial nerve were normal.

Magnetic resonance imaging of his head and spinal cord demonstrated numerous spotty lesions with a marked gadolinium enhancement (**Figure 1**A-C). Computed tomographic scans revealed nodular lesions in both his lungs, parts of which showed increased uptake rates of [^{18}F]-fluorodeoxyglucose (FDG) by positron emission tomography (Figure 1D and E). Video-assisted thoracoscopic biopsy of his left lung revealed infiltrates predominantly composed of lymphocytes. Immunohistochemical staining for CD3 and CD20 showed the predominance of T cells and a few B cells, respectively. In situ hybridization revealed positivity for the EBV-encoded viral RNA in a few lymphocytes (**Figure 2**), confirming the diagnosis of grade 1-2 LYG.

Although various therapeutic options, including whole-brain irradiation, were considered, we thought that less toxic therapeutic approaches were more appropriate for grade 1-2 LYG. Because the neoplastic B cells expressed CD20, the patient was treated with rituximab (375 mg/m^2, once weekly) for 4 weeks. Magnetic resonance images of his head and spinal cord showed marked im-

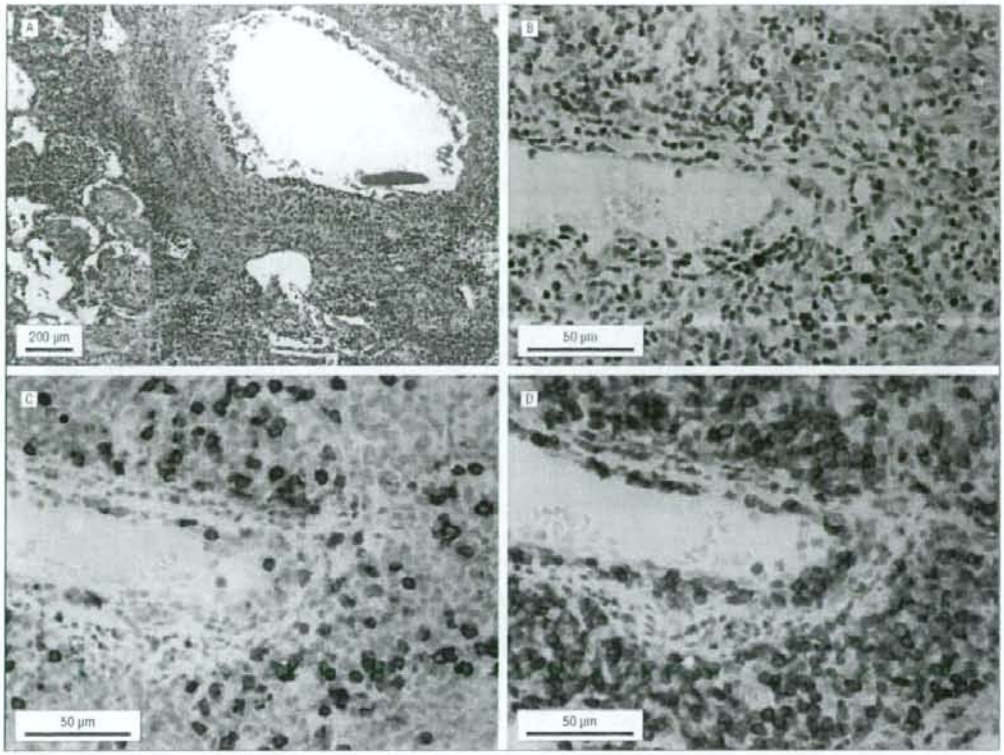

Figure 2. Histopathologic examination of the lung specimen. A, Lymphocytes infiltrate the regions around the bronchi and blood vessels (hematoxylin-eosin). The infiltrates are predominantly small lymphocytes admixed with histiocytes and occasionally large, atypical lymphoid cells, which are angiocentric and angioinvasive, thus destroying the blood vessels. B, Some of the lymphocytes are positive for Epstein-Barr virus–encoded viral RNA. C and D, CD20-positive B cells (C) are surrounded by a large number of CD3-positive T cells (D).

provement of the lesions 1 month after the treatment (**Figure 3**A and B) compared with the lesions in the images obtained before the treatment (Figure 1B and C), followed by further improvement of the lesions 8 months after the treatment (Figure 3C and D). The lesions in the lungs were hardly detected in the computed tomography scans 4 months after the treatment. His pain in his shoulders, back, and hips disappeared. His gait improved and he was able to walk without a cane for several hundred meters. For 18 months, his condition remained stable without recurrence.

COMMENT

In this patient presenting with slowly progressive spastic paraparesis, numerous spotty lesions were observed in the CNS and lungs. The lesions showed contrast enhancement with gadolinium and FDG accumulation, and biopsy of the lesions in the left lung confirmed the diagnosis of LYG.

The definitive diagnosis of LYG is difficult, partly because of its rarity. The radiographic findings of the patient showing numerous granulomatous lesions in the CNS and lungs are highly suggestive of LYG[3] (Figure 1). [^{18}F]-fluorodeoxyglucose accumulation in these lesions further confirmed the diagnosis.[3]

A characteristic clinical feature of the patient was mild neurological signs of spastic paraparesis (he could walk even on admission) despite the striking radiographic findings. Consistent with mild neurological signs, only mild deteriorations in electrophysiological studies were observed in the patient. Such features are sometimes observed, for instance, in miliary tuberculosis involving the CNS. These features can also suggest the possibility of LYG.

Although the prognosis of LYG is variable, the median survival of patients with LYG has been shown to be less than 2 years, and CNS involvement, observed in about 30% of patients with LYG,[1] indicates poor prognosis. Although aggressive therapies, including chemotherapy, radiotherapy, and stem cell transplantation, have been conducted, no satisfactory standard treatment has been established for the treatment of LYG. Epstein-Barr virus–positive B cell infiltration has been established as a pathognomonic feature of LYG. Since then, several reports on treatments with rituximab, with or without

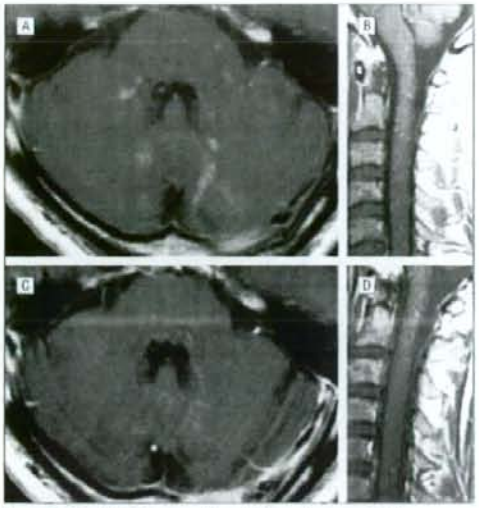

Figure 3. T1-weighted images with gadolinium enhancement of the cerebellum, pons, and cervical cord after treatment. A and B, The pons (A) and cerebellum (B) 1 month after treatment. C and D, The pons (C) and cerebellum (D) 8 months after treatment.

chemotherapy or radiotherapy, have been made.[1-6] Only 1 report on a patient with CNS LYG treated with rituximab alone[3] showed clinical remission for more than 36 months. Although approximately 1% of rituximab seems to pass through the blood-brain barrier and the effects of rituximab on CNS lesions are disputable,[6] our patient responded well to rituximab therapy without any adverse effects and his condition remained stable for 18 months, thus strongly suggesting the efficacy of rituximab monotherapy as the initial therapy for low-grade CNS LYG.

Accepted for Publication: September 16, 2007
Correspondence: Shoji Tsuji, MD, PhD, Department of Neurology, Graduate School of Medicine, The University of Tokyo, 7-3-1 Hongo, Bunkyo-ku, Tokyo 113-8655, Japan (tsuji@m.u-tokyo.ac.jp).
Author Contributions: Drs Ishiura and Morikawa equally contributed to this work. *Study concept and design:* Ishiura, Hamada, Kwak, and Tsuji. *Acquisition of data:* Ishiura, Morikawa, Hamada, Watanabe, Kako, Shibahara, Akahane, Goto, Kwak, Kurokawa, and Tsuji. *Analysis and interpretation of data:* Ishiura, Hamada, Chiba, Motokura, Hangaishi, Shibahara, Akahane, Goto, Kwak, and Tsuji. *Drafting of the manuscript:* Ishiura, Morikawa, Hamada, Goto, Kwak, and Tsuji. *Critical revision of the manuscript for important intellectual content:* Hamada, Watanabe, Kako, Chiba, Motokura, Hangaishi, Shibahara, Akahane, Goto, Kwak, Kurokawa, and Tsuji. *Obtained funding:* Morikawa and Goto. *Administrative, technical, and material support:* Shibahara, Akahane, Kwak, and Tsuji. *Study supervision:* Hamada, Watanabe, Hangaishi, Goto, Kwak, Kurokawa, and Tsuji.
Financial Disclosure: None reported.

REFERENCES

1. Rao R, Vugman G, Leslie WT, Loew J, Venugopal P. Lymphomatoid granulomatosis treated with rituximab and chemotherapy. *Clin Adv Hematol Oncol*. 2003; 1(11):658-660.
2. Sebire NJ, Haselden S, Malone M, Davies EG, Ramsay AD. Isolated EBV lymphoproliferative disease in a child with Wiskott-Aldrich syndrome manifesting as cutaneous lymphomatoid granulomatosis and responsive to anti-CD20 immunotherapy. *J Clin Pathol*. 2003;56(7):555-557.
3. Zaidi A, Kampalath B, Peltier WL, Vesole DH. Successful treatment of systemic and central nervous system lymphomatoid granulomatosis with rituximab. *Leuk Lymphoma*. 2004;45(4):777-780.
4. Jordan K, Grothey A, Grothe W, Kegel T, Wolf HH, Schmoll HG. Successful treatment of mediastinal lymphomatoid granulomatosis with rituximab monotherapy. *Eur J Haematol*. 2005;74(3):263-266.
5. Patsalides AD, Atac G, Hedge U, et al. Lymphomatoid granulomatosis: abnormalities of the brain at MR imaging. *Radiology*. 2005;237(1):265-273.
6. Rubenstein JL, Combs D, Rosenberg J, et al. Rituximab therapy for CNS lymphomas: targeting the leptomeningeal compartment. *Blood*. 2003;101(2):466-468.

THE JOURNAL OF COMPARATIVE NEUROLOGY 511:155–172 (2008)

High-Affinity Na^+/K^+-Dependent Glutamate Transporter EAAT4 Is Expressed Throughout the Rat Fore- and Midbrain

ANN MASSIE,[1] LIESELOTTE CNOPS,[2] ILSE SMOLDERS,[1] ROBERT McCULLUMSMITH,[3] RON KOOIJMAN,[4] SHIN KWAK,[5] LUTGARDE ARCKENS,[2] AND YVETTE MICHOTTE[1]*

[1]Department of Pharmaceutical Chemistry and Drug Analysis, Research Group of Experimental Pharmacology, Vrije Universiteit Brussel, 1090 Brussels, Belgium
[2]Laboratory of Neuroplasticity and Neuroproteomics, Katholieke Universiteit Leuven, 3000 Leuven, Belgium
[3]Department of Psychiatry, University of Alabama at Birmingham, Birmingham, Alabama 35294
[4]Department of Pharmacology, Vrije Universiteit Brussel, 1090 Brussels, Belgium
[5]Department of Neurology, Division of Neuroscience, Graduate School of Medicine, University of Tokyo, Tokyo 113, Japan

ABSTRACT

Excitatory amino acid transporter 4 (EAAT4), a member of the high-affinity Na /K -dependent glutamate transporter family, is highly enriched in Purkinje cells of the cerebellum, although it is not restricted to these cells. The detailed expression of EAAT4 protein in different adult rat fore- and midbrain regions was examined. Despite moderate expression levels compared with the cerebellum, EAAT4 protein was omnipresent throughout the fore- and midbrain. With antibodies raised against the N-terminal mouse EAAT4 sequence, the highest protein expression levels were observed in the substantia nigra pars compacta, ventral tegmental area, paranigral nucleus, habenulo-interpeduncular system, supraoptic nucleus, lateral posterior thalamic nucleus, subiculum, and superficial layers of the superior colliculus. Relatively high levels of EAAT4 protein were also detected in the hippocampal principal cells, in the glutamatergic, γ-aminobutyric acid (GABA)ergic, dopaminergic and most likely cholinergic cells of all nuclei of the basal ganglia, and in neurons of layers II/III and V of the cerebral cortex. The expression of EAAT4 was confirmed at the mRNA level in some important fore- and midbrain structures by in situ hybridization and reverse transcriptase-polymerase chain reaction (RT-PCR) and estimated to range from 6.7 to 1.6% of the amount in the cerebellum as measured by real-time PCR. J. Comp. Neurol. 511:155–172, 2008.

Indexing terms: EAAT4; fore- and midbrain; distribution; immunohistochemistry; real-time PCR; in situ hybridization

High-affinity Na /K -dependent glutamate transporters are responsible for the reuptake of synaptically released glutamate, the major excitatory neurotransmitter in the central nervous system (CNS), into glial cells or neurons. Five different excitatory amino acid transporters (EAATs) have been cloned so far (Saier, 1999; Slotboom et al., 1999): GLAST (Storck et al., 1992; Tanaka, 1993), GLT-1 (Pines et al., 1992), and EAAC1 (Kanai and Hediger, 1992), corresponding to human EAAT1, -2, and -3, respectively, EAAT4 (Fairman et al., 1995), and EAAT5 (Arriza et al., 1997). Through the proper functioning of these glutamate transporters, glutamatergic neurotransmission is carefully regulated and excitotoxicity is prevented (for review, see Danbolt, 2001). This regulation also includes control over the extent of glutamate spillover and ensuing activation of extrasynaptic targets at excita-

Grant sponsor: FWO-Flanders; Grant numbers: 1.5.143.07N, postdoctoral fellowships (to A.M. and I.S.); and research assistant (to L.C.); Grant sponsor: the Vrije Universiteit Brussel.

*Correspondence to: Yvette Michotte, Ph. D., Department of Pharmaceutical Chemistry and Drug Analysis, Research Group of Experimental Pharmacology, Vrije Universiteit Brussel, Laarbeeklaan 103, 1090 Brussels, Belgium. E-mail: ymichot@vub.ac.be

Received 21 December 2005; Revised 24 August 2006; Accepted 11 July 2008

DOI 10.1002/cne.21823

Published online in Wiley InterScience (www.interscience.wiley.com)

tory synapses (Bergles et al., 1999). In addition, glutamate transporters also behave as glutamate-gated chloride channels, a property that is particularly prominent in EAAT4 and EAAT5 (Fairman et al., 1995; Vandenberg et al., 1995; Wadiche et al., 1995a,b; Arriza et al., 1997; Torres-Salazar and Fahlke, 2007).

Originally, the five members of this transporter family were thought to have not only a distinct regional but also a distinct cellular distribution pattern. GLAST and GLT-1 were reported to be confined to glial cells (Rothstein et al., 1994; Torp et al., 1994; Chaudhry et al., 1995; Lehre et al., 1995). EAAC1 and EAAT4 were considered to be strict neuronal transporters (Rothstein et al., 1994; Yamada et al., 1996; Furuta et al., 1997). However, this interpretation was challenged by several reports, and it soon became clear that the subdivision of glutamate transporters into "glial" and "neuronal" was no longer tenable (however, for ease this subdivision is still generally used). GLT-1 is expressed in neurons of cortical and hippocampal culture (Mennerick et al., 1998; Wang et al., 1998). Also, in vivo, GLT-1, as well as its splice variants, can be expressed by neurons (Rauen and Kanner, 1994; Schmitt et al., 1996; Torp et al., 1996; Berger and Hediger, 1998; Berger et al., 2005; Chen et al., 2002, 2004). EAAT4 expression has been reported to be enriched in astrocytes of mouse spinal cord and forebrain (Hu et al., 2003) as well as in rat retinal astrocytes (Ward et al., 2004). Very recently, Liang et al. (2008) described the presence of the mRNA of all EAATs (i.e., EAAT1–5) in astrocyte cultures. Moreover, glia were reported to have the potential to upregulate EAAT4 after traumatic brain injury (Yi et al., 2007). EAAT5, thought to be primarily neuronal, is predominantly expressed in the retina (Arriza et al., 1997) and will therefore not be discussed in further detail.

As for the regional distribution pattern, GLAST immunoreactivity (IR) is known to be highly abundant in cerebellar Bergman glia (Lehre et al., 1995; Lehre and Danbolt, 1998; Attwell, 2000), whereas GLT-1, which is responsible for the bulk of glutamate removal, is highly expressed in astrocytes of the cerebral cortex and hippocampus (Lehre et al., 1995). EAAC1 expression within the CNS has been described in the cerebral cortex, hippocampus, and basal ganglia.

It is commonly accepted that EAAT4 is largely confined to Purkinje cells of the cerebellum, with little or no expression in forebrain regions (Yamada et al., 1996; Bar-Peled et al., 1997; Furuta et al., 1997; Itoh et al., 1997; Nagao et al., 1997; Tanaka et al., 1997; Dehnes et al., 1998; Inage et al., 1998). However, Furuta et al. (1997) have reported very low expression levels of EAAT4 protein in the forebrain and more particularly in the cerebral cortex, hippocampus, and some basal ganglia nuclei. Also, McCullumsmith and Meador-Woodruff (2002) detected EAAT4 mRNA in the striatum of human subjects. Recently, we described the expression of this glutamate transporter in more detail in neurons of the cerebral cortex of cat and mouse (Massie et al., 2001). The presence of EAAT4 in the cerebral cortex has been confirmed at the mRNA (Ward et al., 2004) as well as the protein level (Hu et al., 2003). Nevertheless, the expression level in the cerebral cortex has been estimated to be only approximately 3% that of the cerebellum (Ward et al., 2004). More recently, EAAT4 has also been described to be expressed in photoreceptors and astrocytes of the retina (Ward et al., 2004; Pignataro et al., 2005). Thus, it is becoming more and more clear that EAAT4 is more widespread in distribution than was initially thought. In addition, several recent studies report changes in the expression levels of EAAT4 mRNA and/or protein in various fore-and midbrain regions of various brain pathologies (McCullumsmith and Meador-Woodruff, 2002; Rakhade and Loeb, 2008; Yi et al., 2007).

To our knowledge, this is the first report describing in detail the cellular and regional distribution of EAAT4 protein and mRNA throughout the rat fore- and midbrain. By using an antibody raised against the N-terminal mouse EAAT4 sequence (Yamada et al., 1996), as well as a staining protocol ensuring optimal permeability of cells for the antibodies, EAAT4 protein could be clearly observed in neurons throughout the fore- and midbrain, notwithstanding the manifestly higher levels in the Purkinje cell layer of the cerebellum. In addition, the presence of EAAT4 mRNA in the fore-and midbrain was confirmed by using reverse-transcriptase-polymerase chain reaction (RT-PCR) and in situ hybridization. The expression level of EAAT4 mRNA relative to the cerebellum was determined for the cerebral cortex, hippocampus, and striatum by using real-time PCR.

MATERIALS AND METHODS

Animals

Protocols for animal experiments described in this study were carried out according to national guidelines on animal experimentation and were approved by the Ethical Committee for Animal Experimentation of the Faculty of Medicine and Pharmacy of the Vrije Universiteit Brussel.

All animals used for this study were housed under standard laboratory conditions. Eight adult male Wistar rats (weighing 250–275 g) were sacrificed for the immunohistochemical study, six for the Western blotting, and three for the RT-PCR and real-time PCR experiments.

Mice bearing heterozygous null mutations for EAAT4 were a gift of Dr. K. Tanaka (Huang et al., 2004). Breeding with these mice resulted in litters containing EAAT4$^{+/+}$, EAAT4$^{+/-}$, and EAAT4$^{-/-}$ mice. Four 12-week-old male mice of each genotype were used for this study.

Western blotting

After rats or mice were injected with a lethal dose of pentobarbital, i.p. (Nembutal, Sanofi sante, Brussels, Belgium), brains were immediately dissected. A small tissue sample (± 4 mm^3) was collected from the cerebral cortex, striatum, hippocampus, and cerebellum, snap-frozen in dry ice-cooled 2-methylbutane (−60°C), and stored at 70°C until use.

Protein extraction and Western blotting were performed as described before (Massie et al., 2003). Tissue was homogenized in 2% sodium dodecyl sulfate (SDS; Polylab, Antwerp, Belgium), 60 mM Tris base (ICN Biomedicals, Aurora, OH), pH 6.8, 100 mM dithiothreitol (DTT; Merck Eurolab, Leuven, Belgium), and 1 mM EDTA (Merck Eurolab). After incubation for 30 minutes at 37°C, samples were processed four times through 20-gauge needles and then through a 26-gauge needle, spun at 10,000*g* at 4°C (Eliasof et al., 1998), and immediately boiled for 10 minutes. Supernatants were stored at −70°C. Protein concentrations were determined by using a modified Bradford method (Qu et al., 1997). Equal concentrations of protein

(1.6 μg/lane) were loaded for all forebrain regions; for the cerebellum, four times less protein was loaded.

Proteins were separated by SDS-polyacrylamide gel electrophoresis (PAGE; 4–12% gel; Invitrogen, Groningen, The Netherlands) under reducing conditions and transferred to a polyvinylidene fluoride membrane (Sequi-Blot PVDF Membrane, Bio-Rad Laboratories, Nazareth, Belgium) by using an Xcell II Blot module (Novex, Invitrogen). Nonspecific binding was blocked by incubating the membrane for 1 hour at room temperature in 5% dried milk (ECL blocking agent, GE Healthcare, Roosendaal, The Netherlands). Blots were incubated overnight at 4°C with the immunoaffinity-purified polyclonal antibodies to EAAT4, raised in rabbit against the N-terminal mouse sequence (MSSHGNSLFLRESGAGGGCL; 760 μg/ml; diluted 1:4,000; kindly provided by Dr. M. Watanabe; same batch as in Yamada et al., 1996). The next day, after incubation with horseradish-peroxidase-conjugated anti-rabbit antiserum (1:2,000; Dako, Glostrup, Denmark), immunoreactive proteins were visualized by using enhanced chemiluminescence (ECL; ECLplus kit, GE Healthcare). All washing and dilution steps were performed with Tris-saline (0.01 M, pH 7.4). The MultiMark Multi-Colored Standard (Novex, Invitrogen) was used as molecular weight standard. Negative controls included omission of the immunoaffinity-purified antibody and the secondary antibody, respectively.

Immunohistochemistry

Rats or mice were deeply anesthetized with an overdose of Nembutal, i.p., and transcardially perfused with a physiological solution followed by freshly depolymerized 4% paraformaldehyde (Sigma-Aldrich, St. Louis, MO) in 0.15 M phosphate-buffered saline (PBS; pH 7.42). Brains were removed and postfixed in the same fixative overnight, rinsed in tap water for 24 hours, and stored in 0.015 M PBS at 4°C. Free-floating 50-μm frontal and sagittal sections were made with a vibratome and stored in serial order in 0.015 M PBS at 4°C.

All rinsing steps and incubations of the staining procedure were performed in Tris-saline (0.01 M, 0.05% Triton X-100 [Sigma-Aldrich], pH 7.4) or in 0.015 M PBS, always at room temperature, unless mentioned otherwise, and under gentle agitation. All results shown and discussed were obtained with the Triton X-100-containing staining protocol unless otherwise noted. Incubation steps were separated by three rinsing steps of at least 5 minutes. The sections underwent a permeabilizing treatment consisting of incubation in 0.1% trypsin (Fluka, Buchs, Switzerland) for 1 hour at 37°C prior to a blocking step with normal goat serum (Chemicon, Temecula, CA, diluted 1:5, 45 minutes). Thereafter the sections were incubated with the primary EAAT4 antibodies (diluted 1:2,000; Yamada et al., 1996) for 2 days. On the third day the sections were processed by the avidin-biotin method by using a Vectastain ABC kit (Vector, Burlingame, CA), and immunoreactivity was visualized, after a final rinsing step with acetate buffer, by using the glucose oxidase-diaminobenzidine-nickel method (Shu et al., 1988). Sections were mounted on poly-L-lysine-coated slides, dehydrated through alcohol, cleared with xylene, and coverslipped with Coverquick (Labonord, Templemars, France). Negative controls consisted of the omission of the primary and secondary antibodies, respectively.

Photomicrographs were made of the stained sections, and brightness and contrast were adapted by using Adobe Photoshop 7.0.

Laser microdissection (LMD)

After the brain was snap-frozen, 14-μm sections were cut on a cryostat and mounted on home-made glasses that were covered with a poly-ethylene naphtalate (PEN) foil and exposed to UV radiation for 30 minutes prior to use. Glasses were placed in a Leica AS LMD system (Leica, Leitz Instruments, Heidelberg, Germany) with the section facing downward. After adjusting intensity, aperture, and cutting velocity, the pulsed UV laser beam was carefully directed along the borders of the fasciculus retroflexus of several serial sections by using the 4× objective. The area cut fell by forces of gravity alone into a plastic tube cap placed directly underneath the section. The tube cap was filled with lysis solution. Tissue collection was verified by inspecting the tube cap under higher magnification.

RT-PCR

Total RNA was extracted from tissue samples of the fasciculus retroflexus, collected by the LMD technique, as well as manually isolated tissue samples from cryosections of the cerebellum, cerebral cortex, hippocampus, and striatum, by using the Versagene total RNA purification kit (Gentra Systems, Big Lake, MN). RT-PCR was performed according to the instructions of the manufacturer (GeneAmp® RNA PCR kit from Applied Biosystems, Foster City, CA). For the reverse transcription oligo(dT) primers were used. The EAAT4-specific primers used for PCR amplification were designed according to the known rat sequence of EAAT4 (GenEmbl. u89608; Lin et al., 1998; upstream primer: 5′-GGAGACTGTGCCTGTACCTGG-3′, downstream primer: 5′-GCAGAGCTGGAAGAGGTACCC-3′, corresponding to nucleotides 906–926 and 1,299–1,319 respectively; Eurogentec, Seraing, Belgium). A total of 40 reaction cycles (95°C 1 minute, 60°C 1 minute, 70°C 1 minute) was preceded by 1 cycle starting at 95°C for 10 minutes to activate the polymerase enzyme (AmpliTaq® Gold DNA polymerase, 2.5 U/100 μl; Applied Biosystems) and concluded by a termination step at 70°C for 10 minutes. As negative control the cDNA in the reaction mixture was substituted by water.

Amplified products were analyzed by horizontal agarose gel electrophoresis and visualized by ethidium bromide staining. A 100-bp ladder (Invitrogen) was used as molecular weight reference.

Real-time PCR

Total RNA was extracted, and, after biophotometric analysis (Eppendorf, VWR International, Leuven, Belgium), RT was performed as described above on mRNA samples of identical quantity. Primers and probes were designed by using the Primer Express Program (Applied Biosystems), based on the rat sequence of EAAT4 (GenEmbl. u89608; forward primer: 5′-TTGCGCCTGCAGACCAT-3′; reverse primer: 5′-AGCGCTGACTGTGAGCAAGA-3′; Taqman probe: 5′-CGCTTCCTGCGCCGAAATGC-3′) and GAPDH (GenEmbl. NM017008; forward primer: 5′-TGCCTGGATCCCTAAAGAGACA-3′; reverse primer: 5′-CGCGATATTCAATTGGATACACA-3′; Taqman probe: 5′-CCATTTCCAAGACTGACAGCCCCAGA-3′). Primers were obtained from Eurogentec, and FAM-TAMRA Taqman probes were purchased from Applied Biosystems.

PCR was performed on the cDNA samples in a 25-µl reaction volume of 1× Taqman Universal PCR Master Mix (Applied Biosystems) with primers at a final concentration of 300 nM and probes of 200 nM, using the ABI Prism 7000 Sequence Detection System. Standard curves were generated by running serial dilutions (1:2) of control cDNA in duplicate for each gene. Target samples were run in triplicate on the same well-plate under standard amplification settings (1 cycle of 50°C for 2 minutes, 1 cycle of 95°C for 10 minutes, 40 cycles of 95°C for 15 seconds and 60°C for 1 minutes).

Data were analyzed with ABI Prism 7000 SDS software (version 1.1). EAAT4 quantities were normalized to GAPDH, an endogenous control, to account for variability in the initial concentration of mRNA in the samples and to compensate for differences in conversion efficiency of the RT reaction. Amounts of transcripts in the cerebral cortex, striatum, hippocampus, and fasciculus retroflexus were expressed relative to the cerebellum which was set as the calibrator (=100%). To confirm reproducibility, real-time PCR was performed twice on each rat (n = 3).

In situ hybridization

After rats were injected with a lethal dose of Nembutal, i.p., brains were immediately dissected and snap-frozen in dry ice-cooled 2-methylbutane (−60°C) and then stored at −80°C until use. In situ hybridization experiments were performed as described by McCullumsmith and Meador Woodruff (2002). To generate a subclone for riboprobe synthesis, we amplified a unique region of EAAT4 (U89608, 576–959) from a rat cDNA brain library (Edge-Biosystems, Gaithersburg, MD) by using PCR. Amplified cDNA segments were extracted (QIAquick Gel Extraction kit; Qiagen, Valencia, CA), subcloned (Zero Blunt TOPO PCR cloning kit; Invitrogen, Carlsbad, CA), and confirmed by nucleotide sequencing (Thermo Sequenase Radiolabeled Termination Cycle Sequencing kit; USB, Cleveland, OH). Riboprobes were synthesized by using 100 µCi of dried [^{35}S]-UTP, 2.0 µl 5X transcription buffer, 1.0 µl 0.1 M DTT, 1.0 µl each of 10 mM ATP, CTP, and GTP, 2.0 µl linearized plasmid DNA, 0.5 µl RNAse inhibitor, and 1.5 µl SP6 or T7 RNA polymerase, and incubated for 2 hours at 37°C. After this incubation, 1.0 µl DNAse (RNAse free) was added and incubated for 15 minutes at room temperature. The reaction mixture was separated through spin columns (Micro Bio-Spin P-30 Tris Chromatography Columns, Bio-Rad, Richmond, CA), and the purified fraction was eluted. DTT was added to each fraction to a final concentration of 0.01 M.

Slides were removed from −80°C storage, fixed in 4% (wt/vol) formaldehyde at room temperature for 1 hour, and briefly washed in 2X SSC (standard saline citrate: 300 mM NaCl/30 mM sodium citrate, pH 7.2) three times. The slides were then placed in 0.1 M triethanolamine (pH 8.0)/acetic anhydride (400:1 vol/vol) with stirring for 10 minutes at room temperature. The final wash was in 2X SSC buffer for 10 minutes followed by dehydration in graded ethanol washes and air drying. A coverslip containing the [^{35}S]-radiolabeled riboprobe diluted 5 × 10^6 cpm in 0.1 ml per slide of hybridization buffer (50% formamide, 10% dextran sulfate, 3X SSC, 50 mM Na_2HPO_4, pH 7.4, 1X Denhardt's solution [0.02% poliviny pyrrolidone, 1.02& Ficoll, 0.02% bovine serum albumin], 100 µg/ml yeast tRNA) and 0.01 M DTT was placed on each slide. Slides were then placed in a covered tray with filter paper saturated with 50% formamide buffer and incubated at 55°C overnight. Sense and antisense probes were tested to confirm specificity. After 16 hours of hybridization, the coverslips were removed and the slides were washed in 2X SSC for 2 minutes and again in 2X SSC for 15 minutes, and then immersed in RNAse A (200 µg/ml in 10 mM Tris-HCl pH 8.0/0.5 M NaCl) for 30 minutes at 37°C. The slides then underwent washes through descending concentrations of SSC, to a final concentration of 0.1X SSC at 55°C for 1 hour twice. Sections were finally dehydrated in graded ethanol washes, air-dried, and exposed to Kodak BIOMAX MR film (Kodak, Rochester, NY) for 3 months. All sections were run in the same experiments to eliminate interassay variability. Neighboring sections were stained with Richardson's methylene blue-azure II Nissl stain (Richardson et al., 1960). Digital photomicrographs of the Nissl-stained sections were made by using the Leica IM50 software. Brightness and contrast were adapted by using Adobe Photoshop 7.0.

Fig. 1. **A:** Western blot analysis with the EAAT4 antibodies on protein extracts from rat cerebellum (Cb), cerebral cortex (Cx), hippocampus (Hc), and striatum (Str). In each lane one band could be detected with a molecular weight of approximately 68 kDa. **B:** Western blotting on homogenates of cerebellar (Cb) and cerebral cortex (Fb) of EAAT4 heterozygous (+/−) and homozygous (−/−) mice and their wild-type (+/+) littermates. **C:** Immunohistochemical staining of frontal sections of EAAT4 $^{+/+}$ and EAAT4 $^{-/-}$ mouse brain by using the EAAT4 antibody. Scale bar = 1 mm in C.

RESULTS

Specificity of the antibodies

Western blotting was used to investigate the specificity of the antibody in recognizing EAAT4 in four principal rat brain regions. Proteins were extracted from the cerebral cortex (Cx), the striatum (Str), the hippocampus (Hc), and the cerebellum (Cb) of the rat. Incubation of the blotting membrane with the EAAT4 antibody that recognizes the N-terminus of EAAT4 resulted for all protein samples in the detection of a specific band with a molecular weight of approximately 68 kDa, corresponding to the molecular weight of EAAT4 (Fig. 1A).

We observed a difference of a few kDa between the molecular weight of the immunoreactive bands of the cerebellum and the forebrain regions, the latter being a few kDa higher than the former (Fig. 1A). However, exposing the light-sensitive film for a longer period of time to the membrane revealed a second band for the cerebellum with

the same molecular weight as the bands of the forebrain regions (data not shown). Because of the very high intensity of the lower band, these two bands appear as one broad and intense band. Possibly, the appearance of this double band can be explained by post-translational modifications, the higher band corresponding to a more glycosylated and/or phosphorylated form of EAAT4 (Massie et al., 2001). If phosphorylations are mostly localized to the N-terminus of the protein, it might make the epitope of the antibodies less accessible, explaining why this higher molecular weight band is less easily detected, compared with the lower molecular weight band. At the same time, this might explain why bands are faint and fuzzy in forebrain regions where we only detected this higher molecular weight band (Fig. 1A). For all conditions, when higher protein concentrations were loaded, a smear of higher molecular weight bands became noticeable. These bands have been described abundantly in the literature for EAAT4 (Hu et al., 2003) as well as for the other glutamate transporter subtypes (Danbolt et al., 1990; Haugeto et al., 1996) as being multimers of the transporter protein. Omitting the primary antibodies resulted in a blank lane (data not shown).

Specificity of the antiserum was further confirmed by Western blotting and immunohistochemistry on samples of the cerebellum and cerebral cortex of mice bearing heterozygous or homozygous null mutations for EAAT4 and their wild-type littermates. When comparing samples of cerebral cortex with the same amount of protein, the concentration of the 68 kDa band in the EAAT4 $^{+/-}$ samples is markedly reduced compared with the wild-type samples, whereas in the EAAT4 $^{-/-}$ mice this band is absent (Fig. 1B, lower arrow). Similar observations were made in the cerebellum, where the 68-kDa band was reduced in heterozygous mice and completely absent in EAAT4 $^{-/-}$ mice. However, in EAAT4 $^{+/-}$ and EAAT4 $^{-/-}$ mice we detected immunoreactive bands with a molecular weight slightly higher than the 68-kDa band found in WT mice (Fig. 1B, upper arrow). This immunoreactive band was completely absent in the homogenates of their WT littermates.

We speculate that insertion of the neoTK targeting vector in the coding region of exon 8 leads to partial transcription of this vector and as a consequence the translation of low levels of a larger protein of which the N-terminal region is identical to the N-terminal part of EAAT4 and thus still recognized by the antibody. This idea is in line with the detection of a faint immunoreactive signal in forebrain slices of EAAT4 $^{-/-}$ mice after immunohistochemical staining in comparison with EAAT4 $^{-/-}$ mice (Fig. 1C). In samples of the cerebellum, the difference in concentration between the larger protein and the WT protein is much more pronounced, because the former is only visible after prolonged exposure of the membrane to the light-sensitive film (data not shown).

Immunohistochemical distribution of EAAT4

Overview. In general, EAAT4-positive neurons could be detected throughout the whole rat brain, with the most intense staining in the cerebellum (Fig. 3C,D). In the fore- and midbrain (Figs. 3–6), the strongest signal was present in the subiculum (S), substantia nigra pars compacta (SNc), ventral tegmental area (VTA), medial habenular nucleus (MHb), fasciculus retroflexus, interpeduncular nucleus (IP), supraoptic nucleus, paranigral nucleus, lateral posterior thalamic nucleus (LPMC), and superficial and zonal layers of the superior colliculus (SC) (Figs. 4–6, Table 1). A relatively strong labeling could also be detected in layers II/III and V of the cerebral cortex (Fig. 3A,B), the principal cells of the hippocampal formation (Fig. 4), and the basal ganglia (Fig. 6, Table 1).

Overall, when Triton X-100 was included in rinsing and incubation steps (Tris-saline or PBS + 0.3% Triton), immunopositive neurons were much more abundantly present compared with staining without Triton (rinsing and incubation with PBS) (Fig. 3A,B). Moreover, in sections treated with Triton X-100, EAAT4-IR was clearly present in the cytoplasm (Figs. 2, 3B). This finding suggests that the antigenic sites in the cytoplasm are less reachable compared with those from EAAT4 proteins in cell membranes and dendrites. Conversely, in accordance with the observations of Dehnes et al. (1998), in the cerebellar Purkinje cells, we detected intracellular staining without Triton X-100, probably because of the higher concentrations of EAAT4 in the cerebellum compared with the fore- and midbrain. As was proposed for EAAC1, this deviating localization might imply that EAAT4 can be rapidly mobilized from the cytoplasm to the plasma membrane, resulting in rapid changes in EAAT4-surface expression near the synapse (Davis et al., 1998; Conti et al., 1998; Kugler and Schmitt, 1999).

Besides the intense somatodendritic labeling, which manifests as a uniform dark staining, we could also detect a punctate or granular staining (Fig. 2). This granular staining is prominent in the neuropil and dendrites but also in the cell bodies. Some cell bodies are defined only by these granules (Fig. 2D,E), whereas others show a dark homogeneous staining of some parts of the cell body or the whole cell body and are additionally covered by these granules (Fig. 2C).

In general, glial labeling was very faint and could be observed in several white matter regions of the brain, in ependymal cells and tanycytes lining the lateral and third ventricle as well as in the choroid plexus (Table 1). The typical arrangement of the glial cells in rows, as observed in the corpus callosum, leads us to think that we are staining oligodendrocytes rather than astrocytes. This glial labeling is not the result of aspecific staining because it was absent from the stained EAAT4 $^{-/-}$ sections.

Cerebellar cortex. In the cerebellar cortex, Purkinje cells were intensely immunoreactive, as was the molecular layer. When Triton X-100 was not used for incubating and rinsing the sections (Fig. 3C,D), we could clearly distinguish the dendrites of the Purkinje cells in the molecular layer (Mo). At higher power magnification we could differentiate small dots at the end of the branches of the dendrites, probably representing the dendritic spines (Fig. 3D, arrows), in accordance with the observations of Nagao et al. (1997) and Dehnes et al. (1998). When Triton X-100 was included in the staining protocol, we observed a very dense and homogeneous punctate staining of this layer (data not shown). With neither protocol could we detect EAAT4 labeling in the granular layer (Gr) or the white matter.

Septal and basal forebrain regions. Despite the ubiquitous distribution of EAAT4 protein in the basal forebrain and the septal complex, EAAT4 expression was rather low to moderate, compared with other fore- and

TABLE 1 Distribution of EAAT4 Immunoreactivity in the Rat Brain[1]

Brain region	EAAT4 Neuropil	EAAT4 Neurons
Cerebellar cortex		
Purkinje cells		+
Molecular layer		
Granular layer		
Septal and basal forebrain regions		
Lateral septal nucleus		
Medial septal nucleus	+	+
Bed nucleus of the stria terminalis		+
Nucleus of the vertical limb of the diagonal band		
Nucleus of the horizontal limb of the diagonal band		+
Substantia innominata		+
Septohippocampal nucleus		
Septofimbral nucleus		
Septohypothalamic nucleus		
Triangular septal nucleus		+
Subfornical organ		
Cerebral cortex		
Isocortex		
Layer I		
Layer II/III		
Layer IV		
Layer V	+	
Layer VI	+	
Allocortex		
Piriform		
Cingulate		
Insular		
Perirhinal	+	+
Retrosplenial		+
Entorhinal		
Hippocampal formation		
Subiculum	+ +	+ +
CA1-3		
Pyramidal cell layer	+	+ + +[3]
Stratum oriens	+	+[3]
Stratum radiatum		+
Dentate gyrus		
Hilus		+[3]
Stratum granulosum		+ +
Stratum moleculare	+	
Dorsal thalamus and metathalamus		
Posterior thalamic nuclear group		+
Anteroventral nucleus	+	+
Anterodorsal nucleus	+	+
Anteromedial nucleus		
Laterodorsal nucleus		
Ventrolateral nucleus		
Ventromedial nucleus		+
Ventroposteromedial and lateral nucleus	+	+
Mediodorsal intermediodorsal nucleus		
Dorsolateral nucleus		+
Lateral posterior nucleus	+	+
Mediodorsal nucleus		+
Centrolateral nucleus	+	+
Centromedial nucleus	+	+
Parafascicular nucleus	+	+
Anterior paraventricular nucleus	+ + +	+ + +
Posterior paraventricular nucleus	+	+
Ventral paraventricular nucleus		
Ventral subpiriform nucleus		+[4]
Dorsal endopiriform nucleus		
Reticular nucleus		+
Paracentral nucleus		
Gelatinosa nucleus		+
Rhomboid nucleus		+
Reuniens nucleus		
Perifascicular nucleus		
Posterior intralaminar thalamic nucleus	+	
Subparafascicular thalamic nucleus		
Suprageniculate thalamic nucleus		+
Ventral medial geniculate nucleus		
Dorsal medial geniculate nucleus		+
Medial medial geniculate nucleus		
Dorsal lateral geniculate nucleus		
Ventral lateral geniculate nucleus		
Epithalamus		
Medial habenula		
Lateral habenula		+

TABLE 1 (Continued)

Brain region	EAAT4 Neuropil	EAAT4 Neurons
Hypothalamic and preoptic region		
Preoptic area		
Suprapetic nucleus		
Anteroventral preoptic nucleus		
Magnocellular preoptic nucleus		+ +
Anterior hypothalamic area		+ +
Lateral hypothalamic area		
Paraventricular hypothalamic area	+	+
Dorsal hypothalamic area	+	+
Ventromedial nucleus	+	+
Dorsomedial nucleus	+	
Dorsal hypothalamic nucleus	+	+ +[3]
Periventricular nucleus	+	+
Tuber cinereum area		+
Medial tuberale nucleus		+ + +[3]
Arcuate nucleus		+
Perifornical nucleus		
Periventricular hypothalamic nucleus		+ +
Zona incerta		
Subincertal nucleus		
Amygdaloid complex		
Cortical nucleus		
Amygdalapiriform transition		+
Amygdalohippocampal nucleus		
Anterior amygdaloid area		+
Anterior cortical nucleus		+
Central nucleus		
Basomedial nucleus		
Basolateral nucleus	+	+
Lateral nucleus		
Medial nucleus	+	
Intercalated nuclei amygdala	+	+
Basal ganglia, ventral thalamus and associated nuclei		
Nucleus accumbens shell		+
Nucleus accumbens core		+ +
Striatum (caudate-putamen)		+ +
Globus pallidus	+ +	+
Subthalamic nucleus	+	+ +
Substantia nigra pars compacta		+ + +
Substantia nigra pars reticulata		+ +
Substantia nigra pars lateralis	+	+ + +
Entopeduncular nucleus	+	
Fundus striati		
Ventral pallidum		
Ventral tegmental area		+
Mesencephalic regions		
Interpeduncular nucleus		
Rostral subnucleus		
Caudal subnucleus		
Rostrolateral subnucleus		+
Dorsomedial subnucleus		+
Apical subnucleus	+	
Peripeduncular nucleus	+	+
Anterior pretectal nucleus	+	
Posterior pretectal nucleus		+
Nucleus optic tract		
Deep mesencephalic nucleus		+ +
Red nucleus		
Parazigral nucleus		+ + +
Central gray		
Superior colliculus		
Zonal layer		
Superficial gray layer	+	+
Optic nerve layer		+ +
Intermediate gray layer		+
Intermediate white layer		+
Oculomotor nucleus		+
Interstitial nucleus		
Rostral linear nucleus raphe		+
Caudal linear nucleus raphe		+ + +
Lateral terminal nucleus accessory optic tract		+
Prerubral field		
White matter	Glia	
Fasciculus retroflexus	+	
Corpus callosum	+	
Anterior commissure	+	
Fornix	+	
Fimbria hippocampus	+	
Internal capsule	+	
Optic tract	+	
Mammillothalamic tract	+	
Stria medullaris thal		
Commissure superior colliculus		
Cerebral peduncle	+	
Brachium superior colliculus		
Ventral hippocampal commissure		

[1]Relative intensities of neuropil staining and relative number of labeled neurons: low labeling; low to moderate labeling; moderate to high labeling; high labeling; no labeling.
[2]Very intensely stained neurons.
[3]Solitary, intensely stained neurons with immunopositive dendrites, intermingled with a larger number of faintly stained cell bodies.
[4]Somatodendritic staining.

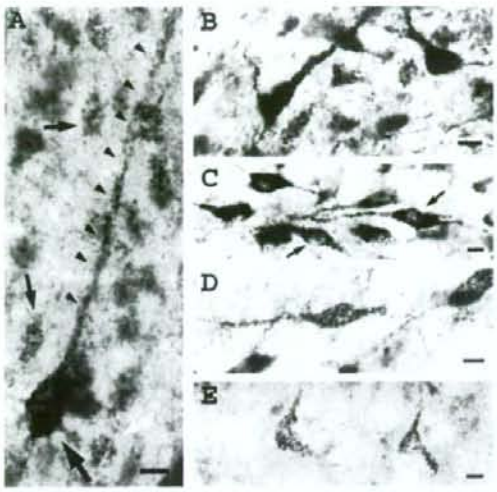

Fig. 2. Detail of EAAT4-immunoreactive neurons in the cerebral cortex (A), VTA (B,C), SNc (D), and prerubral field (E) after staining in the presence of Triton X-100. **A:** Pyramidal neurons of layer V of the cerebral cortex are intensely and homogeneously stained (large arrows). Dendrites of these neurons are visualized as an alignment of immunoreactive puncta (arrowheads). Intermingled with the intensely stained pyramidal neurons, faintly stained neurons could be seen that are composed of labeled granules (small arrows). Also neuropil staining consists of EAAT4-positive granules. **B–D:** EAAT4-IR in the VTA (B,C) and SNc (D). Besides very intensely and homogeneously stained neurons (B, arrow), we could detect neurons with nuclei devoid of this homogeneous and intense IR, although covered with immunoreactive puncta (C, arrows). Some of the neurons, as well as their dendrites, are defined only by these immunoreactive puncta (D). **E:** Two faintly stained neurons located in the prerubral field show a punctate labeling. Scale bar = 10 μm in A–E.

midbrain regions (Table 1). We observed relatively strong labeling in the subfornical organ (SFO) (data not shown).

Cerebral cortex. EAAT4-immunoreactive neurons were detected in layers II–VI throughout all subdivisions of the cerebral cortex, the isocortex, and the allocortex (Fig. 3A,B). In general, the strongest labeling was observed in the tightly packed cells of layers II/III as well as in the sparsely distributed, large multipolar pyramidal neurons of layer V (Figs. 2A, 3A,B). Apical dendrites of the pyramidal neurons of layer V could be followed into layer II (Figs. 2A, 3A,B). With the Triton-free staining protocol, IR could be detected predominantly in the somatodendritic compartment of neurons of layers II/III and layer V (Fig. 3A). In Triton-exposed material, cells were abundantly present in all layers of the cerebral cortex, except for layer I (Fig. 3B). The pyramidal cells of layer V are still more intensely stained and the lamination pattern still emerges because of the stronger neuropil staining in layers II/III and V compared with the other layers.

Hippocampal formation. Figure 4 illustrates how IR was readily apparent in the subiculum (S), in principal and nonprincipal cells of the CA1–3 fields of Ammon's horn (hippocampus proper or cornu Ammonis), in the stratum granulosum (sg) of the dentate gyrus (DG), and in scattered larger cells with neuronal morphology in the hilus (H). Because axonal fibers and synaptic terminals were not stained, it was impossible to categorize EAAT4-positive interneurons in terms of the locations of their axonal projections.

On the whole, in the hippocampal formation we observed a punctate or granular, yet very dense and intense, staining of the cell somata (Fig. 4H–J).

In the subiculum (S; Fig. 4A,B), EAAT4-immunoreactive neurons in the pyramidal cell layer (pyr) were plentiful and intensely stained. Dendrites of all neurons could be followed into the molecular layer, where they formed a dense meshwork.

In the dentate gyrus (Fig. 4C), EAAT4-positive neurons were abundantly present in the stratum granulosum (sg) whereas significant numbers of large multipolar cells could be observed in the hilus (H) and a few cells in the stratum moleculare (sm). Although it is a simple matter to identify most hippocampal principal cells anatomically, the principal cells of the dentate hilus (i.e., the glutamatergic mossy cells; Soriano and Frotscher, 1994; Wenzel et al., 1997) are intermingled with hilar interneurons (Amaral, 1978) and therefore cannot be differentiated by using standard staining methods. Nevertheless, neurons within the hilar region showed an intense punctate labeling in addition to the faint homogeneous staining of the cell body (Fig. 4D).

Within CA1–3, EAAT4 expression was observed in the somata and initial part of the apical dendrites of pyramidal cells (Fig. 4E–J). Labeling of the dendrites was manifested as an alignment of a large number of immunopositive puncta (Fig. 4H). Immunoreactive neurons were more densely packed in a more orderly fashion in the stratum pyramidale (sp) of CA1 (Fig. 4E,H) compared with CA2 and CA3 (Fig. 4F,G, I, J). Scattered multipolar neurons were found in the stratum oriens (so) and stratum radiatum (sr).

Dorsal thalamus, metathalamus, and epithalamus. On the whole, EAAT4 expression within the thalamic nuclei was moderate relative to the general staining intensity in the fore- and midbrain, with a few exceptions as described below. Very high expression levels could be detected in the MHb (Fig. 5A). When the remaining regions of the forebrain were still immunonegative, staining of the MHb was already intense, as well as staining of the IP (Fig. 5E,F) and the axon bundle connecting both nuclei, namely, the fasciculus retroflexus (fr; Fig. 5B–E). For the MHb we detected a predominant neuropil staining. In the lateral habenular nucleus (LHb) neuropil staining was significantly lower. However, in this nucleus immunoreactive neurons were abundantly present, contrary to the MHb (Fig. 5A, Table 1). A very intense neuropil staining could be observed in the caudal (IPC) and rostrolateral subnucleus (IPRL) of the IP, whereas staining of the rostral (IPR), dorsomedial, and apical subnuclei was rather moderate (Fig. 5F, Table 1). In frontal (Fig. 5A,B) as well as sagittal (Fig. 5D,E) sections, the striate immunoreactive signal of the fasciculus retroflexus could be traced from the departure of the axon bundle in the habenular nuclei (Hb) until arrival in the IP. On the course from the Hb to the IP, branching of the fibers was observed only once (Fig. 5B, arrows).

Hypothalamus and preoptic region. In general, relatively high expression levels of EAAT4 protein could be observed within the hypothalamic region (Table 1). The different nuclei that compose the hypothalamus could be

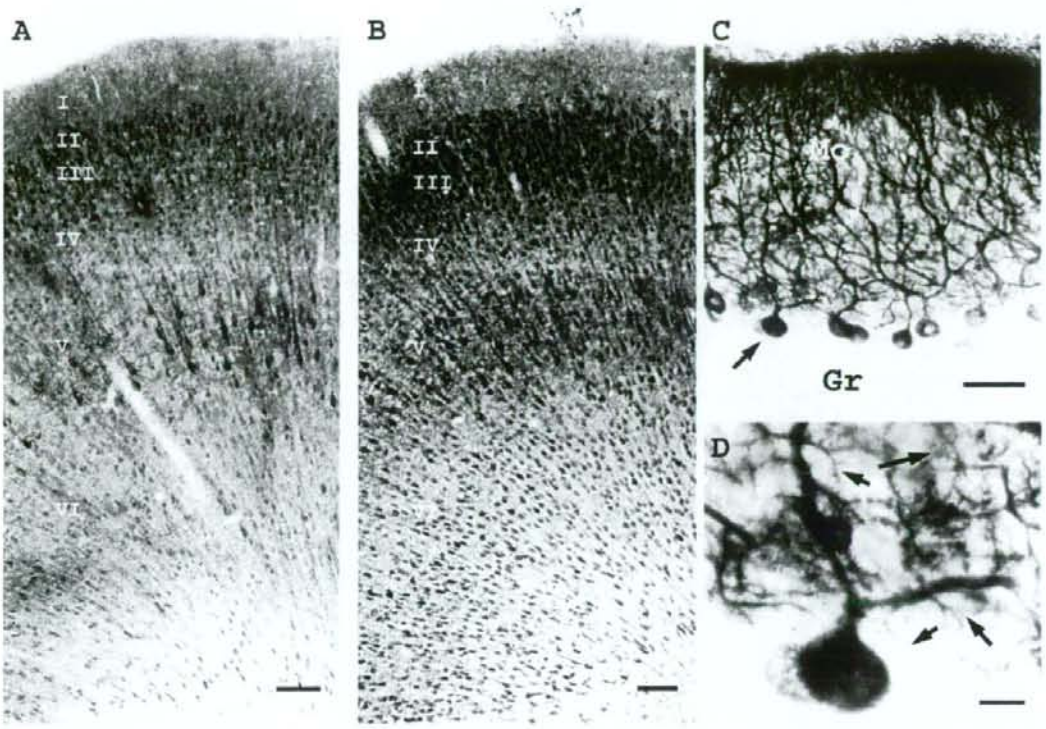

Fig. 3. EAAT4-IR in cerebral (A,B) and cerebellar (C,D) cortex using the EAAT4 antiserum in the presence (B) or absence (A,C,D) of Triton X-100. **A,B:** Immunopositive neurons could be detected in all layers of the cerebral cortex. When Triton was used (B) in the staining protocol, the number of immunopositive cells was significantly higher compared with Triton-free stainings (A). Apical dendrites of the pyramidal neurons in layer V could be followed into layer II. **C:** EAAT4 labeling was highly enriched in the Purkinje cells (arrow) and in the molecular layer (Mo). The granular layer (Gr) was devoid of IR. **D:** Detail of an immunostained Purkinje cell and dendrites in the Mo. Small dots at the ends of the branches are suggestive of dendritic spines (arrows). Scale bar 100 μm in A,B; 50 μm in C; 10 μm in D.

distinguished very easily after staining. Within each nucleus, EAAT4-immunoreactive cell bodies were homogeneously distributed. Except for the dorsal hypothalamic nucleus, in which large intensely immunoreactive multipolar neurons were sparsely distributed and in which immunoreactivity expanded into the dendrites, immunostained cell bodies were rather small and densely packed. Here too, the majority of the cell bodies consisted of a collection of immunoreactive puncta or granules (data not shown).

Amygdaloid complex. In the majority of the nuclei constituting the amygdala, a moderate to relatively high expression level of EAAT4 protein could be observed (Table 1).

Basal ganglia and associated nuclei. EAAT4-positive neurons could be detected in all structures of the

Fig. 4. Expression profile of EAAT4 throughout the hippocampal formation, as visualized by using the staining protocol including Triton X-100. **A:** Overview of EAAT4-IR in a frontal section at Bregma −5.2. **B:** Relatively high expression levels of EAAT4 could be detected in neurons located in the pyramidal layer (pyr) of the subiculum (S). Immunoreactive apical dendrites of the pyramidal neurons expanded into the molecular layer (ml). **C:** Neurons of the stratum granulosum (sg) of the dentate gyrus (DG) were quite intensely stained, as were scattered neurons in the hilus (H). **D:** A higher power photomicrograph of labeled neurons in the hilar region demonstrates the granular staining. **E–J:** Also, the principal cells in the stratum pyramidale (sp) of CA1 (E,H), CA2 (F,I), and CA3 (G,J) show a dense granular EAAT4 labeling (arrows), extending into the initial part of the apical dendrites (H, arrowheads), as well as sparse nonprincipal cells in stratum oriens (so) and stratum radiatum (sr). Abbreviations: Ctx, cerebral cortex; Ent, entorhinal cortex; fr, fasciculus retroflexus; LPMC, mediocaudal lateral posterior thalamic nucleus; LT, lateral terminal nucleus accessory optic tract; MG, medial geniculate nucleus; pol, polymorphic layer; SC, superior colliculus; sm, stratum moleculare; SNc, substantia nigra pars compacta; SNr, substantia nigra pars reticulate; VTA, ventral tegmental area. Scale bar 500 μm in A; 100 μm in B,C; 50 μm in E–G; 25 μm in D; 10 μm in H–J.

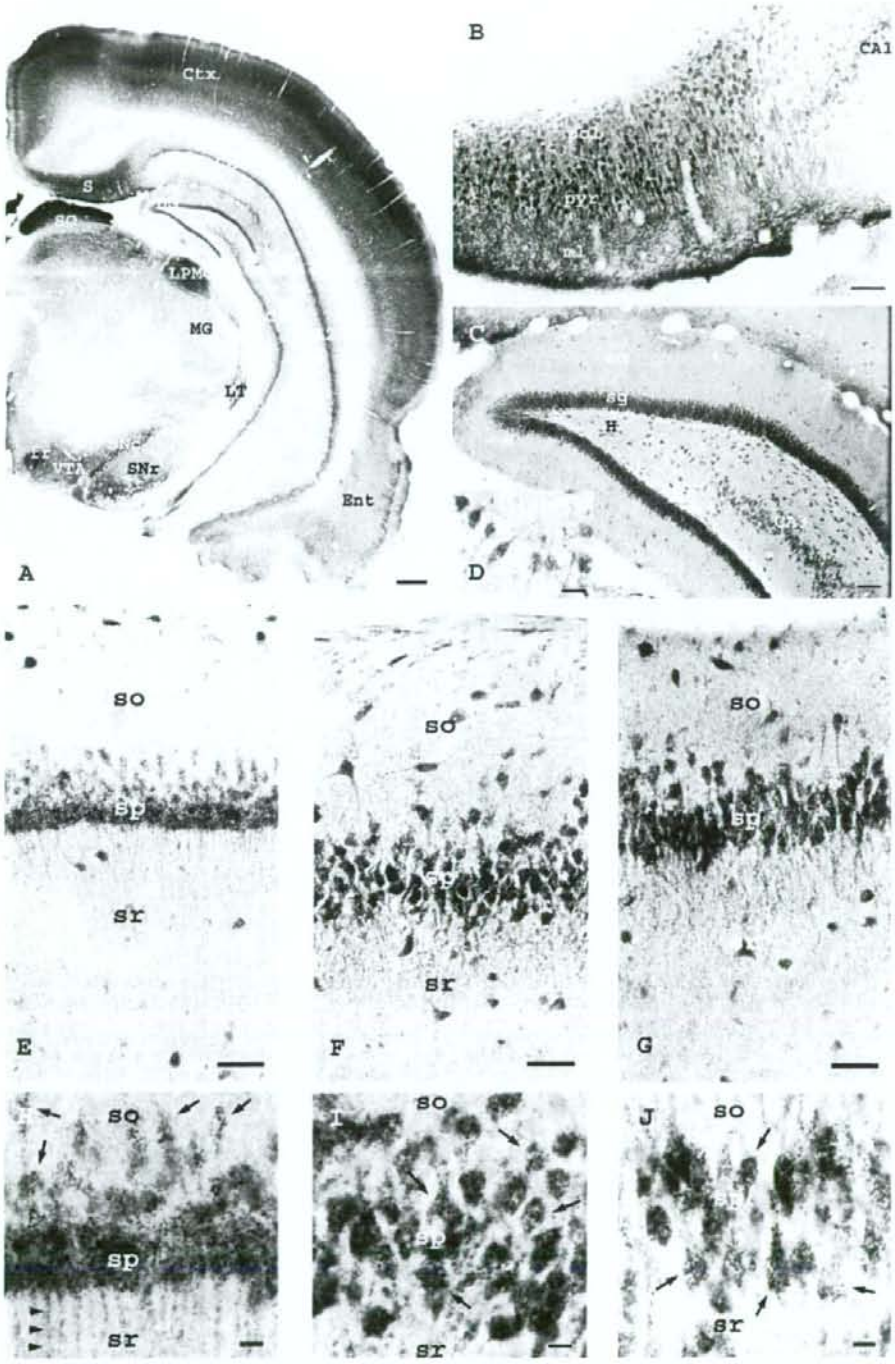

Figure 4

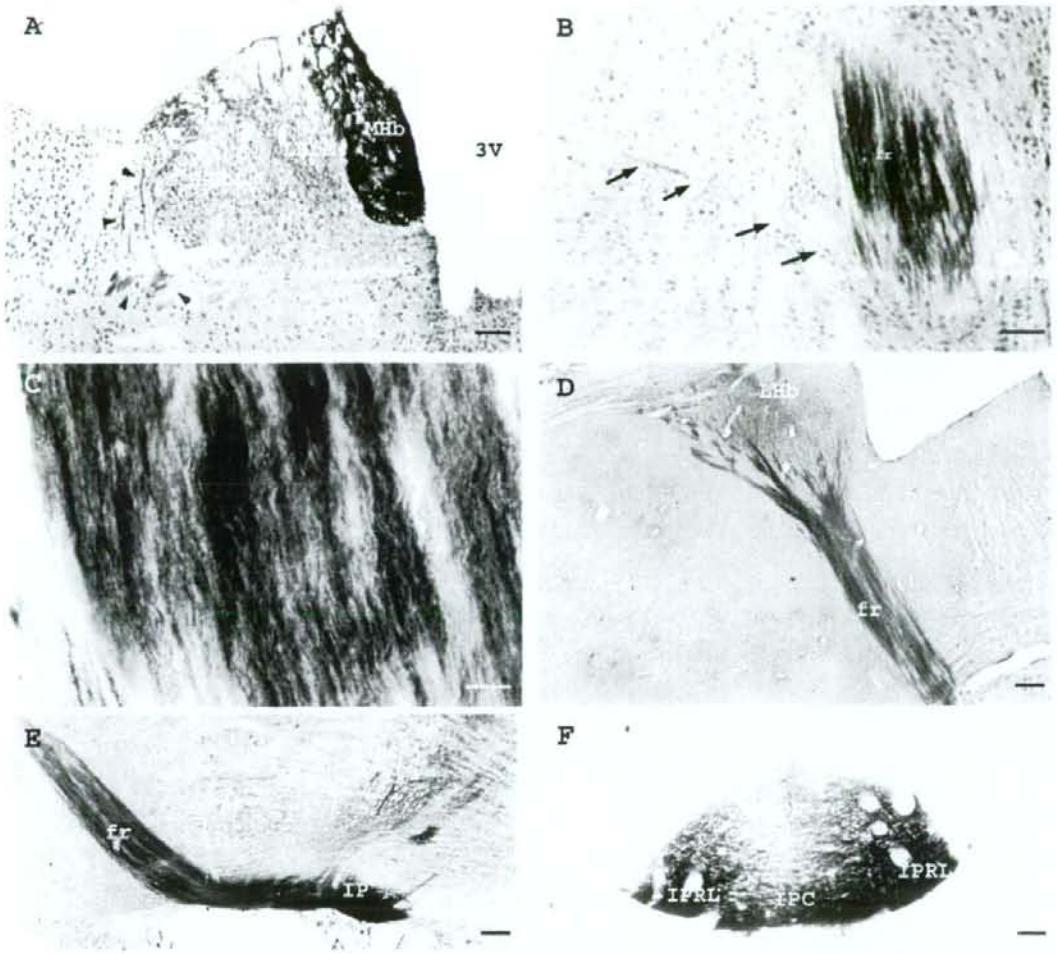

Fig. 5. EAAT4-IR in the presence of Triton X-100, in frontal (A–C,F) and sagittal (D,E) sections through the habenular nuclei (Hb; A,D), the fasciculus retroflexus (fr; B–E), and interpeduncular nucleus (IP; E,F). **A:** In the medial habenular nucleus (MHb) immunoreactivity was confined to the neuropil, whereas in the lateral habenular nucleus (LHb) EAAT4 labeling could be observed in neuronal cell bodies. Arrowheads point to fibers of the fasciculus retroflexus, originating in the habenular nuclei. **B:** An intense striate-like labeling in the fasciculus retroflexus can be seen. Arrows point to an immunoreactive branch of the main bundle. **C:** In more detail, this striate labeling consists of immunoreactive punctae. **D,E:** Sagittal sections demonstrate the course of the fasciculus retroflexus, starting in the Hb and arriving in the IP. **F:** Intense staining was also seen in the rostrolateral subnucleus of the IP (IPRL) and caudal nucleus of the IP (IPC), whereas staining was less intense in the rostral nucleus of the IP (IPR). Abbreviations: 3V, third ventricle; LHbL, lateral part of the lateral Hb; LHbM, medial part of the lateral Hb. Scale bar = 100 μm in A,F; 50 μm in B; 25 μm in C; 200 μm in D,E.

basal ganglia, i.e., the striatum (Fig. 6A), globus pallidus (Fig. 6B), subthalamic nucleus (STN; Fig. 6C), substantia nigra (SN; Fig. 6D), and entopeduncular nucleus (EP; Fig. 6E), with the most intensely stained neurons being present in the SNc (Figs. 4A, 6D). In the VTA, a basal ganglia-related structure, labeling was as intense as in the SNc (Figs. 4A, 6F).

In the striatum (Fig. 6A), immunoreactive intermediate-sized neurons were abundantly present, indicating that EAAT4 is present in most of the γ-aminobutyric acid (GABA)ergic efferent spiny neurons that account for 96% of the total neuronal population of the striatum (Ribak et al., 1979; Kita and Kitai, 1988). These immunoreactive cells are homogeneously distributed without any correspondence with patches (striosomes)/matrix compartments (Gerfen, 1992; Hiroi, 1995). EAAT4 labeling was observed exclusively in cell bodies, dendrites being devoid of any staining. In between these intermediate-sized neurons, a few solitary,

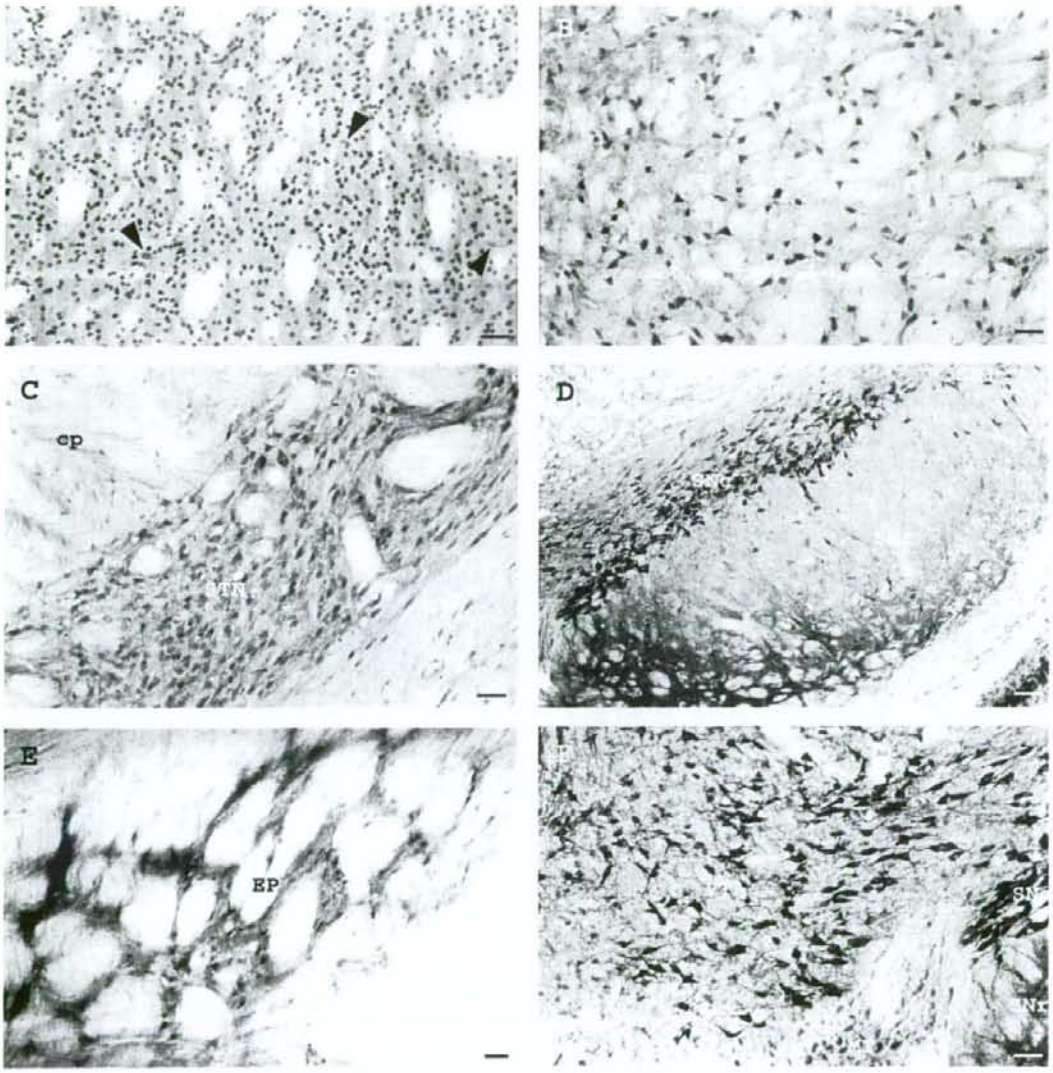

Fig. 6. Immunohistochemical staining in the presence of Triton X-100, illustrating the distribution of EAAT4 throughout the basal ganglia. **A:** Detail of the striatum. In the middle of a large number of homogeneously distributed intermediate-sized neurons, very few, faintly stained large neurons could be distinguished (arrowheads). **B,C:** Detail of the globus pallidus (B) and the subthalamic nucleus (STN; C). EAAT4-immunoreactive neurons were homogeneously distributed. EAAT4 label was present in the cell bodies and dendrites. **D:** A large number of intensely labeled neurons could be seen in the substantia nigra pars compacta (SNc). In the substantia nigra pars lateralis (SNl) cells were less abundant but still intensely stained. Only a few intensely labeled cells were present in the substantia nigra pars reticulata (SNr), in the middle of a number of faintly stained neurons. **E:** In the entopeduncular nucleus (EP), sparse immunoreactive neurons could be visualized in a meshwork of immunoreactive neuropil. **F:** In the VTA intensely and homogeneously stained neurons were abundantly present. Abbreviations: cp, cerebral peduncle; MT, medial terminal nucleus accessory optic tract. Scale bar = 50 μm in A,B,D–F; 100 μm in C.

large, very faintly stained neurons could be detected when Triton X-100 was used (Fig. 6A, arrowhead). These large neurons probably represent the large aspiny cholinergic interneurons of type II (25–35 μm), which account for 1–2% of the total neuron population, because this is the only cell type in the striatum exhibiting this size (Yelnik, 2002). As in the

striatum, in the globus pallidus (Fig. 6B) and STN (Fig. 6C), EAAT4-immunoreactive neurons were homogeneously distributed. Staining was present in cell bodies and, contrary to the striatum, also in dendrites. In the EP, a few immunoreactive neurons could be visualized, whereas neuropil staining was moderate (Fig. 6E).

As for the SNc (Figs. 2D, 6D) and VTA (Figs. 2B,C, 6F), very intensely and homogeneously stained, densely packed neurons were visualized after EAAT4 staining. The nucleus of some immunopositive neurons was devoid of this intense and homogeneous labeling, yet was often covered by a number of immunoreactive puncta (Fig. 2C, arrow). Still other neurons and most of the dendrites were defined only by these immunoreactive puncta (Fig. 2D,E). In the substantia nigra pars laterale (SNl), the staining pattern of the immunoreactive neurons was similar to that of the SNc; however, the density of immunoreactive neurons was significantly smaller compared with the SNc. In contrast, in the substantia nigra pars reticulata (SNr), an occasional intensely stained neuron was present in the middle of a small number of faintly stained neurons, characterized by a punctate labeling (Fig. 6D).

Mesencephalic regions. EAAT4 was omnipresent in the midbrain region. Besides the aforementioned high expression levels in the IP (Fig. 5F) and VTA (Fig. 6F), EAAT4 was also enriched in the superficial layers of the SC (Fig. 4A). The immunoreactive signal in the SC was higher than average, with a very intense neuropil staining in the zonal layer and superficial gray layer. In the optic nerve layer, cell bodies as well as dendrites showed clear EAAT4 labeling.

Reverse transcription polymerase chain reaction

The presence of EAAT4 in the fasciculus retroflexus was further investigated on the mRNA level, given the unexpected abundant occurrence of EAAT4 protein in an axon bundle. After collecting the tissue samples by means of the LMD technique (Fig. 7A–C), making it possible to isolate tissue very precisely from the fasciculus retroflexus without contamination from any other nearby brain tissue, RT-PCR was performed with up- and downstream primers corresponding to rat EAAT4 nucleotide sequences 906–926 and 1,299–1,319, respectively (Lin et al., 1998; Massie et al., 2001). As a control we also included mRNA samples of the cerebellum, cerebral cortex, striatum, and hippocampus. For each condition a fragment was amplified with a length of 414 bp, the expected length based on the known sequence (Fig. 7D). No fragment was amplified when the cDNA in the PCR reaction mixture was replaced by water.

Real-time PCR

In order to estimate tissue expression levels of EAAT4 mRNA, semiquantitative analysis was performed by using real-time PCR. As expected, the cerebellum was found to contain by far the highest levels of EAAT4 mRNA (Fig. 7E). By comparison, after setting the cerebellum as calibrator, the cerebral cortex contained 6.7 ± 1.8%, the hippocampus 2.0 ± 0.4%, the striatum 1.6 ± 0.2%, and the fasciculus retroflexus 4.7 ± 1.8% of the total cerebellar EAAT4 mRNA content (n = 3). These mRNA levels are on the same order of magnitude as those measured by Ward et al. (2004) in the cerebral cortex, i.e. 3.1% relative to the cerebellum.

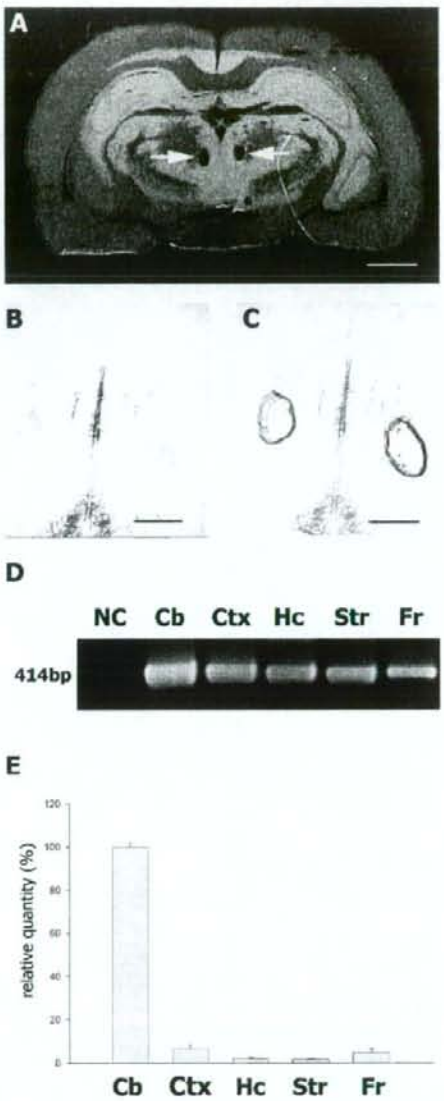

Fig. 7. **A:** Photograph showing a frontal section from which the fasciculus retroflexus (arrows) was bilaterally removed by laser microdissection. **B,C:** Detail of the same section before (B) and after (C) the fasciculus retroflexus was laser-collected. **D:** Conventional end-point RT-PCR with specific primers for EAAT4 on mRNA from the cerebellum (Cb), cerebral cortex (Ctx), hippocampus (Hc), striatum (Str), and laser-captured fasciculus retroflexus (Fr). No band could be detected in the negative control lane (NC), whereas for all other conditions a band of 414 bp was visualized. **E:** Real-time PCR analysis of EAAT4 mRNA expression in rat cerebellum (Cb), cerebral cortex (Ctx), hippocampus (Hc), striatum (Str), and fasciculus retroflexus (Fr). EAAT4 mRNA expression levels were normalized to GAPDH. The amount of transcript in forebrain regions was expressed as mean value (n = 3, ± SD) relative to cerebellum (= 100%). Scale bar = 2 mm in A; 0.5 mm in B,C.

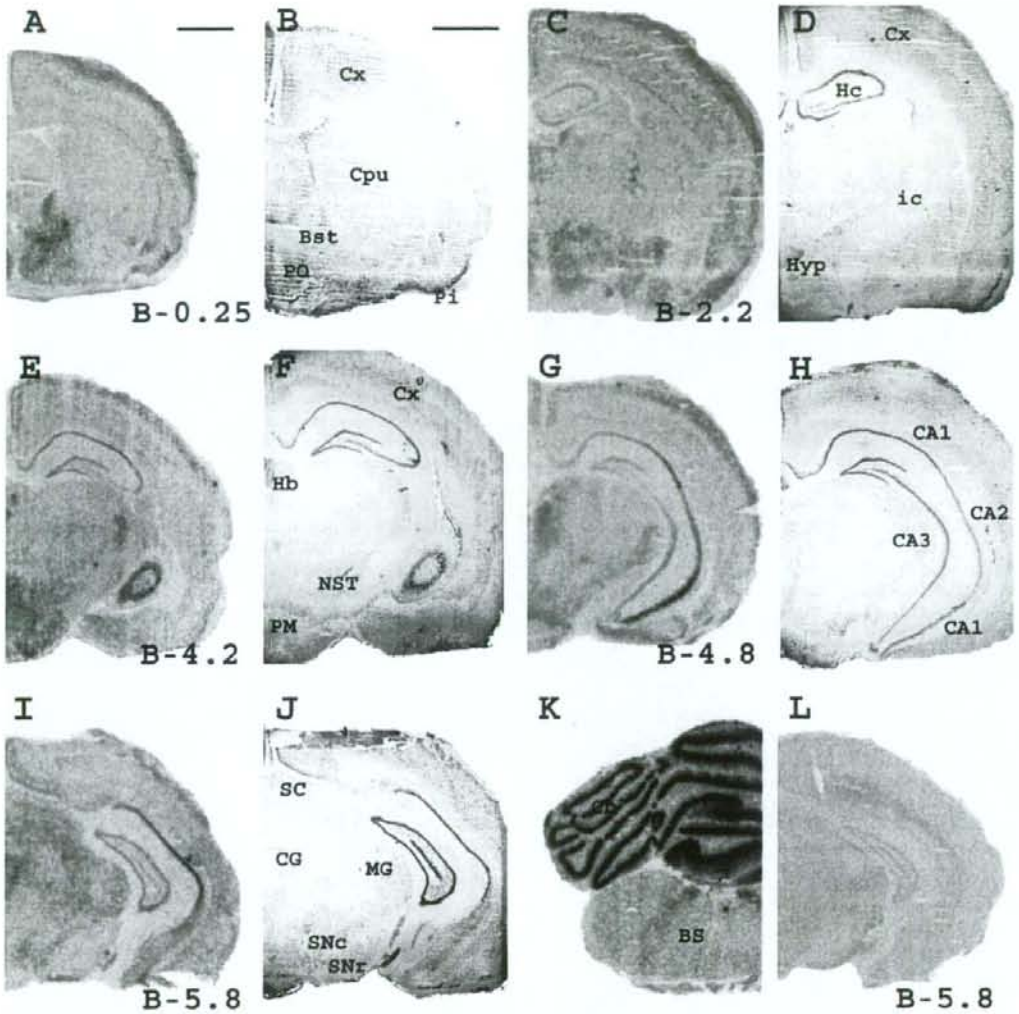

Fig. 8. Distribution of EAAT4 mRNA throughout the fore- and midbrain (A–J) and cerebellum (K). Autoradiograms were generated after in situ hybridization by using EAAT4 ^{35}S-labeled antisense (A,C,E,G,I,K) and sense (L) riboprobes. Neighboring sections were stained with Richardson's methylene blue-azure II Nissl stain (B,D, F,H,J). **A–J:** In the fore -and midbrain, labeling was higher than average in layers II/III and layer V of the cerebral cortex (Cx; A,C,E,G), the substantia nigra pars compacta (SNc; I), the medial geniculate nucleus (MG; I), and the superior colliculus (SC; I). Clear EAAT4 labeling was observed in the preotpic area (PO; A), the bed nucleus of the stria terminalis (Bst; A), piriform cortex (Pi; A), hypothalamic region (Hyp; C), premammillary nuclei (PM; E), the CA1 region of the hippocampus (Hc; G), and the central gray (CG; I). **K:** A very high signal was observed in the cerebellum (Cb). Abbreviations: BS, brainstem; CPu, caudate putamen; Hb, habenular nuclei; ic, internal capsule; NST, subthalamic nucleus; SNr, substantia nigra pars reticulate. Scale bar 2 mm. Scale bar in panel A applies to all in situ hybridization figures (i.e. panel C, E, G, I, K, L); scale bar in B applies to all Nissl stains (i.e. D, F, H, J).

In situ hybridization

As a last verification of the immunohistochemical data for EAAT4, in situ hybridization was performed on sections containing some important brain regions (Fig. 8). EAAT4 mRNA expression was by far highest in the cerebellar cortex (Fig. 8K). As for the cerebral cortex, we could clearly distinguish a layered pattern with the highest signal in layers II/III followed by layer V (Fig. 8A,C,E,G,I). Also, a relatively intense signal was observed in the piri-

form cortex (Fig. 8A,C). As for the hippocampal formation, relatively strong labeling could be seen in all CA regions, with the most intense signal in CA1 and in the dentate gyrus (Fig. 8E,G). Concerning the nuclei of the basal ganglia, high EAAT4 signal was present in the SNc (Fig. 8I). In addition, clear EAAT4 labeling occurred in the preoptic area, the bed nucleus of the stria terminalis, several hypothalamic, amygdaloid, and premammillary nuclei (Fig. 8C,E), in the central gray, and in the intermediate gray layer of the superior colliculus (Fig. 8I). Labeling with the sense probe resulted in a faint background signal (Fig. 8L).

DISCUSSION

In this paper we describe for the first time in detail the widespread distribution of EAAT4 protein throughout the rat fore- and midbrain. EAAT4, which is highly enriched in the Purkinje cells of the cerebellum, was omnipresent in the rat fore- and midbrain, albeit at protein levels significantly lower compared with those in the cerebellum. On the whole, EAAT4-IR was localized not merely in glutamatergic and GABAergic neurons, but also in dopaminergic and probably cholinergic neurons. Besides the neuronal localization of EAAT4 protein, a very faint glial labeling in white matter of several CNS regions as well as in the ventricular walls could be observed. Given the unexpected high expression level of EAAT4 protein in the fasciculus retroflexus, the presence of EAAT4 in this axon bundle was confirmed at the mRNA level and estimated to be 4.7% that of the cerebellum. In addition, the distribution of EAAT4 in the main brain nuclei was confirmed on the mRNA level by using conventional RT-PCR as well as in situ hybridization.

In general, given the presence of the glial glutamate transporters, which are, in most fore- and midbrain regions, responsible for the bulk of glutamate reuptake, and given the low glutamate transport rate of EAAT4 (Torres-Salazar and Fahlke, 2007), we can imagine that the functional significance of EAAT4 in all these regions is not solely linked to glutamate reuptake activity. EAAT4 has large substrate-gated Cl currents that are not coupled to substrate transport. Thus, besides taking up glutamate to terminate glutamate neurotransmission, EAAT4 might also modulate neurotransmission by dampening of neuronal excitability via the substrate-gated anion conductance, without interfering with glutamate homeostasis. In addition, it has been noted that metabotropic glutamate receptor activation is specifically controlled by neuronal glutamate transporters in the cerebellar cortex (Brasnjo and Otis, 2001), and it was suggested by Otis et al. (2004) that this interaction could influence synaptic plasticity in a synapse-specific manner. Moreover, metabotropic glutamate receptors and neuronal glutamate transporters, which are closely associated in the perisynaptic space, can serve together as a physiological mechanism for limiting glutamate spillover from excitatory synapses (Otis et al., 2004). This is further supported by results obtained from EAAT4-deficient mice, indicating that indeed in the cerebellum EAAT4 is responsible for effectively preventing glutamate from spilling over to neighboring synapses (Takayasu et al., 2005).

Unfortunately, all studies on mice lacking EAAT4 are uninformative on brain regions outside the cerebellum (Huang et al., 2004; Takayasu et al., 2005, Yamashita et al., 2006). The reuptake of glutamate by EAAT4 can also have a metabolic role. After being transported into the cell, glutamate can be converted into α-ketoglutarate by glutamic acid decarboxylase and then enter the tricarboxylic acid cycle to produce ATP. The functionality of EAAT4 in the fore- and midbrain is further supported by the observation of Huerta et al. (2006) that the mRNA of the EAAT4-associated interacting proteins KIAA0302 and ARHGEF11 is highly expressed throughout the brain.

In the hippocampal formation, a strong somatodendritic labeling could be observed in the pyramidal cell layer of the subiculum. Also, the pyramidal cell layer of CA1–3 and the granular cell layer of the dentate gyrus showed a staining higher than average. Besides EAAT4, all other glutamate transporter subtypes (Lehre et al., 1995; Kugler and Schmitt, 1999) as well as glutamate receptor subtypes (Monaghan et al., 1989; Petralia and Wenthold, 1992) are expressed throughout the hippocampus, which is not surprising given that the glutamatergic as well as the GABAergic in- and output to all parts of the hippocampal formation is quite abundant (Ottersen and Storm-Mathisen, 1984). Moreover, in the stratum radiatum of CA1, synapses are often found side by side without any intervening glial processes (Harris and Stevens, 1989; Sorra and Harris, 1993; Lehre and Danbolt, 1998), making neuronal glutamate reuptake more important relative to other brain regions (Rothstein et al., 1996).

Concerning the nuclei of the basal ganglia, very strong staining could be observed in the SNc and in the VTA, a basal ganglia-related structure. Neurons from the SNc receive, among other inputs, glutamatergic input from the medial prefrontal cortex, the STN, and the pedunculopontine region. Also the VTA receives glutamatergic input from a number of different brain structures, including the prefrontal cortex (Carr and Sesack, 2000; Sesack and Pickel, 1992; Thierry et al., 1983), the pedunculopontine nucleus (Charara et al., 1996; Kelland et al., 1993), and the bed nucleus of the stria terminalis (Georges and Aston-Jones, 2001, 2002). In the SNc as well as the VTA, EAAT4 is present on dopaminergic neurons. Direct evidence comes from staining performed on rats with 6-OHDA lesions of the medial forebrain bundle. Five weeks after lesioning, a dopaminergic cell loss of 90% can be observed in the SN and VTA (Sarre et al., 2004), which corresponds to the loss of EAAT4-immunoreactive cells that we observe in both nuclei (personal observations). The glutamatergic afferents to the SNc and VTA are probably involved in the regulation of these dopaminergic neurons. Therefore, several glutamate receptor subtypes (*N*-methyl-D-aspartate [NMDA] and non-NMDA) have been found in both brain regions (Fallon and Loughlin, 1995; Kalivas, 1993). For the same reasons it is not surprising that EAAT4 has a high expression level in these neurons.

Regarding the other nuclei of the basal ganglia, as discussed above, we detected a relatively high expression level of EAAT4 in the striatum as well as the STN. Interestingly, both nuclei share common characteristics because they both receive cortical and thalamic afferents (Parent, 1986; Canteras et al., 1990) and project to the pallidum and SN (Parent, 1986; Kita and Kitai, 1987). In GABAergic cells, glutamate taken up by EAAT4 can serve as a precursor for neosynthesis of GABA (Furuta et al., 1997; Seal and Amara, 1999) and thus enhance the inhibitory synaptic strength. In addition, the presence of EAAT4 on striatal neurons might be part of the glutama-

tergic regulation of the dopaminergic activity in the striatum as well as the STN, described by Wüllner et al. (1994) and Ampe et al. (2007), respectively. Small fractions of ionotropic and metabotropic striatal EAA binding sites are located on dopaminergic terminals where they may have a distinct impact on dopaminergic activity. As for the expression of EAAT4 on cholinergic neurons, we might speculate that, again, it is linked to its chloride channel properties, which make it behave, to some extent, as an inhibitory glutamate receptor (Dehnes et al., 1998). In addition, as described above, EAAT4 can transport glutamate into the neuron, which can then serve as an energy source.

A moderate expression level could be observed in the globus pallidus and the EP. In the SNr only very few intensely labeled neurons could be seen intermingled with a moderate number of faintly stained neurons. However, in addition to the GABAergic input provided by the caudate-putamen (Chevalier and Deniau, 1990; Deniau et al., 1978), a prominent glutamatergic innervation of the SNr is provided by fibers of the STN (Hammond et al., 1978; Kitai and Kita, 1987; Nakanishi et al., 1987), and all classes of glutamate receptor subtypes are present in this area (Albin et al., 1992).

EAAT4-IR was very pronounced in the habenulo-interpeduncular system, including the fasciculus retroflexus. Given this unexpected expression of EAAT4 in an axon bundle, we further investigated the presence of EAAT4 here. Real-time PCR revealed a relatively high amount of EAAT4 mRNA in the fasciculus retroflexus compared with the other fore- and midbrain regions examined. Surprisingly, and in sharp contrast to EAAT4, for all other high-affinity glutamate transporters, i.e., GLAST, GLT-1, and EAAC1, the fasciculus retroflexus is devoid of immunolabeling. In addition, the glial glutamate transporters GLAST and GLT-1 are absent from the MHb, whereas EAAC1, like EAAT4, is expressed in this nucleus. However, all glutamate transporters show a considerable expression level in the LHb (personal observations). The MHb contains cholinergic and substance P-containing neurons, the former being crowded in the ventral two-thirds of the nucleus whereas the latter are exclusively localized in the dorsal part (Contestabile et al., 1987). Some neurons of the MHb feature dense glutamatergic innervation (Robertson et al., 1999), and glutamate serves as the excitatory transmitter at MHb-IP synapses (Brown et al., 1983; McGehee et al., 1995). This might explain the very high expression levels of EAAT4 in both aforementioned nuclei as well as the expression of metabotropic glutamate receptors, as reported before by Kinoshita et al. (1998).

The fasciculus retroflexus however, is an axonal tract. Projecting GABAergic neurons from the LHb sent axons through the mantle of the tract to midbrain cell targets (the SN, VTA, and raphe) (Herkenham and Nauta, 1979; Carlson et al., 2000). In contrast, the MHb projects through the core of the tract, corresponding to the cholinergic half of the fasciculus retroflexus (Herkenham and Nauta, 1979; Woolf and Butcher, 1989), to the IP. This part of the fasciculus retroflexus contains the highest concentration of nicotinic receptors in brain (London et al., 1985; Perry and Kellar, 1995). Our staining suggests that the immunoreactive fibers originate in the LHb as well as the MHb. These fibers could be followed until arrival in the IP. We were able to detect branching of the fasciculus retroflexus only once, which is not surprising given the small width of such branches.

The most plausible explanation for the labeling of this axon bundle with the EAAT4 antibodies is that not the axons but the glial processes, which are intimately associated with the axons, contain EAAT4 protein and mRNA.

The faint glial labeling obtained with the EAAT4 antiserum was not restricted to glial cells located in the white matter of several CNS regions. Also, ependymal cells lining the lateral and third ventricle were stained. Hu et al. (2003) detected glial labeling. However, they did not observe colocalization of EAAT4-IR with an oligodendrocyte marker, whereas they did with an astrocyte marker. Our data do not exclude the presence of EAAT4 in astrocytes, although the typical arrangement of the majority of the cells in rows strongly suggests that EAAT4 protein is localized to oligodendrocytes. Also, EAAC1, originally considered to be confined to neurons, was localized to glial cells. In accordance with our data, EAAC1 was expressed in oligodendrocytes of white matter, in ependymal cells, and in epithelial cells of the choroid plexus (Kugler and Schmitt, 1999). In epithelial cells of the choroid plexus no GLAST or GLT-1 could be detected, contrary to the tanycytes and ependymal cells (Berger and Hediger, 2000, 2001). Therefore, the presence of EAAC1 and EAAT4 in the choroid plexus might be important to prevent the passage of glutamate from the blood stream into the cerebrospinal fluid, where the glutamate concentration is very low, as stated by Kugler and Schmitt (1999).

In conclusion, some areas of high EAAT4-IR coincide with target areas of dense glutamatergic innervation, e.g., some corticofugal pathways, as described before for GLAST and GLT-1 (Lehre et al., 1995). However, some areas known to be low in glutamatergic innervation, e.g. globus pallidus, also show a considerable EAAT4 expression level, indeed suggesting that the role of EAAT4 in these regions goes beyond the canonical role of glutamate removal. Thus, whether the functional significance of this widespread distribution of EAAT4 in the fore- and midbrain is related to its re-uptake activities or to possible other functional roles that this transporter can play, on account of its chloride channel properties (Sonders and Amara, 1996; Seal and Amara, 1999) or its close association with metabotropic glutamate receptors (Otis et al., 2004), needs further investigation. After all, besides decreasing the total glutamate concentrations, EAAT4 can also prevent excessive excitation and help membrane repolarization inasmuch as its activation elicits chloride influx and consequent local hyperpolarization (Raiteri et al., 2002). Moreover, the interaction of the neuronal glutamate transporters with the metabotropic glutamate receptors can influence synaptic plasticity as well as limit the glutamate spillover from excitatory synapses, as described for the cerebellum (Otis et al., 2004).

ACKNOWLEDGMENTS

The authors acknowledge Mr. G. De Smet and Ms. R. Vanlaer for excellent technical assistance, Dr. M. Watanabe for providing us with the antibodies, and Dr. K. Tanaka for the EAAT4 mice.

LITERATURE CITED

Albin RL, Marcowier RL, Hollingsworth ZR, Dure LS, Penney JB, Young AB. 1992. Excitatory amino acid binding sites in the basal ganglia of the rat: a quantitative autoradiographic study. Neuroscience 46:35–48.

Amaral DG. 1978. A Golgi study of cell types in the hilar region of the hippocampus in the rat. J Comp Neurol 182:851–914.

Ampe B, Massie A, D'Haens J, Ebinger G, Michotte Y, Sarre S. 2007. NMDA-mediated release of glutamate and GABA in the subthalamic nucleus is mediated by dopamine: an in vivo microdialysis study in rats. J Neurochem 103:1063–1074.

Arriza JL, Eliasof S, Kavanaugh MP, Amara SG. 1997. Excitatory amino acid transporter 5, a retinal glutamate transporter coupled to a chloride conductance. Proc Natl Acad Sci U S A 94:4155–4160.

Attwell D. 2000. Brain uptake of glutamate: food for thought. J Nutr 130:1023S–1025S.

Bar-Peled O, Ben-Hur H, Biegon A, Groner Y, Dewhurst S, Furuta A, Rothstein JD. 1997. Distribution of glutamate transporter subtypes during human brain development. J Neurochem 69:2571–2580.

Berger UV, Hediger MA. 1998. Comparative analysis of glutamate transporter expression in rat brain using differential double in situ hybridization. Anat Embryol (Berl) 198:13–30.

Berger UV, Hediger MA. 2000. Distribution of the glutamate transporters GLAST and GLT-1 in rat circumventricular organs, meninges, and dorsal root ganglia. J Comp Neurol 421:385–399.

Berger UV, Hediger MA. 2001. Differential distribution of the glutamate transporters GLT-1 and GLAST in tanycytes of the third ventricle. J Comp Neurol 433:101–114.

Berger UV, DeSilva TM, Chen W, Rosenberg PA. 2005. Cellular and subcellular mRNA localization of glutamate transporter isoforms GLT1a and GLT1b in rat brain by in situ hybridization. J Comp Neurol 492:78–89.

Bergles DE, Diamond JS, Jahr CE. 1999. Clearance of glutamate inside the synapse and beyond. Curr Opin Neurobiol 9:293–298.

Brasnjo G, Otis TS. 2001. Neuronal glutamate transporters control activation of postsynaptic metabotropic glutamate receptors and influence cerebellar long-term depression. Neuron 31:607–616.

Brown DA, Docherty RJ, Halliwell JV. 1983. Chemical transmission in the rat interpeduncular nucleus in vitro. J Physiol (Lond) 341:655–670.

Canteras NS, Shammah-Lagnado SJ, Silva AB, Ricardo JA. 1990. Afferent connections of the subthalamic nucleus: a combined retrograde and anterograde horseradish peroxydase study in the rat. Brain Res 513: 43–59.

Carlson J, Armstrong B, Switzer III RC, Ellison G. 2000. Selective neurotoxic effects of nicotine on axons in fasciculus retroflexus further support evidence that this is a weak link in brain across multiple drugs of abuse. Neuropharmacology 39:2792–2798.

Carr DB, Sesack SR. 2000. Projections from the rat prefrontal cortex to the ventral tegmental area: target specificity in the synaptic associations with mesoaccumbens and mesocortical neurons. J Neurosci 20:3864–3873.

Charara A, Smith Y, Parent A. 1996. Glutamatergic inputs from the pedunculopontine nucleus to midbrain dopaminergic neurons in primates: *Phaseolus vulgaris*-leucoagglutinin anterograde labeling combined with postembedding glutamate and GABA immunohistochemistry. J Comp Neurol 364:254–266.

Chaudhry FA, Lehre KP, Campagne MV, Ottersen OP, Danbolt NC, Storm-Mathisen J. 1995. Glutamate transporters in glial plasma membranes: highly differentiated localizations revealed by quantitative ultrastructural immunocytochemistry. Neuron 15:711–720.

Chen W, Aoki C, Mahadomrongkul V, Gruber CE, Wang GJ, Blitzblau R, Irwin N, Rosenberg PA. 2002. Expression of a variant form of the glutamate transporter GLT1 in neuronal cultures and in neurons and astrocytes in the rat brain. J Neurosci 22:2142–2152.

Chen W, Mahadomrongkul V, Berger UV, Bassan, M, DeSilva T, Tanaka K, Irwin N, Aoki C, Rosenberg PA. 2004. The glutamate transporter GLT1a is expressed in excitatory axon terminals of mature hippocampal neurons. J Neurosci 24:1136–1148.

Chevalier G, Deniau JM. 1990. Disinhibition as a basic process in the expression of striatal functions. Trends Neurosci 13:277–280.

Contestabile A, Villani L, Fasolo A, Franzoni MF, Gribaudo L, Oktedalen O, Fonnum F. 1987. Topography of cholinergic and substance P pathways in the habenulo-interpeduncular system of the rat. An immunocytochemical and microchemical approach. Neuroscience 21:253–270.

Conti F, DeBiasi S, Minelli A, Rothstein JD, Melone M. 1998. EAAC1, a high-affinity glutamate transporter, is localized to astrocytes and GABAergic neurons besides pyramidal cells in the rat cerebral cortex. Cereb Cortex 8:108–116.

Danbolt NC. 2001. Glutamate uptake. Prog Neurobiol 65:1–105.

Danbolt NC, Pines G, Kanner BI. 1990. Purification and reconstitution of the sodium- and potassium-coupled glutamate transport glycoprotein from rat brain. Biochemistry 29:6734–6740.

Davis KE, Straff DJ, Weinstein EA, Bannerman PG, Correale DM, Rothstein JD, Robinson MB. 1998. Multiple signaling pathways regulate cell surface expression and activity of the excitatory amino acid carrier 1 subtype of Glu transporter in C6 glioma. J Neurosci 18:2475–2485.

Dehnes Y, Chaudhry FA, Ullensvang K, Lehre KP, Storm-Mathisen J, Danbolt NC. 1998. The glutamate transporter EAAT4 in rat cerebellar Purkinje cells: a glutamate-gated chloride channel concentrated near the synapse in parts of the dendritic membrane facing astroglia. J Neurosci 18:3606–3619.

Deniau JM, Hammon C, Riszk A, Feger J. 1978. Electrophysiological properties of identified output neurons of the rat substantia nigra (pars compacta and pars reticulata): evidence for the existence of branched neurons. Exp Brain Res 32:409–422.

Eliasof S, Arriza JL, Leighton BH, Kavanaugh MP, Amara SG. 1998. Excitatory amino acid transporters of the salamander retina: identification, localization and function. J Neurosci 18:698–712.

Fairman WA, Vandenberg RJ, Arriza JL, Kavanaugh MP, Amara SG. 1995. An excitatory amino-acid transporter with properties of a ligand-gated chloride channel. Nature 375:599–603.

Fallon JH, Loughlin SE. 1995. Substantia nigra. In: Paxinos G, editor. The rat nervous system. San Diego: Academic Press. p 215–237.

Furuta A, Rothstein JD, Martin LJ. 1997. Glutamate transporter protein subtypes are expressed differentially during rat CNS development. J Neurosci 17:8363–8375.

Georges F, Aston-Jones G. 2001. Potent regulation of midbrain dopamine neurons by the bed nucleus of the stria terminalis. J Neurosci 21: RC160.

Georges F, Aston-Jones G. 2002. Activation of ventral tegmental area cells by the bed nucleus of the stria terminalis: a novel excitatory amino acid input to midbrain dopamine neurons. J Neurosci 22:5173–5187.

Gerfen CR. 1992. The neostriatal mosaic: multiple levels of compartimental organization. Trends Neurosci 15:133–139.

Hammond C, Deniau JM, Rizk A, Feger J. 1978. Electrophysiological demonstration of an excitatory subthalamonigral pathway in the rat. Brain Res 151:235–244.

Harris KM, Stevens JK. 1989. Dendritic spines of CA1 pyramidal cells in the rat hippocampus: serial electron microscopy with reference to their biophysical characteristics. J Neurosci 9:2982–2997.

Haugeto O, Ullensvang K, Levy LM, Chaudhry FA, Honoré T, Nielsen M, Lehre KP, Danbolt NC. 1996. Brain glutamate transporter proteins form homomultimers. J Biol Chem 271:27715–27722.

Herkenham M, Nauta WJH. 1979. Efferent connections of the habenular nuclei in the rat. J Comp Neurol 187:19–48.

Hiroi N. 1995. Compartmental organization of calretinin in the rat striatum. Neurosci Lett 197:223–226.

Hu W-H, Walters WM, Xia X-M, Karmally SA, Bethea JR. 2003. Neuronal glutamate transporter EAAT4 is expressed in astrocytes. Glia 44:13–25.

Huang YH, Dykes-Hoberg M, Tanaka K, Rothstein JD, Bergles DE. 2004. Climbing fiber activation of EAAT4 transporters and kainate receptors in cerebellar Purkinje cells. J Neurosci 24:103–111.

Huerta I, McCullumsmith RE, Haroutunian V, Giménez-Amaya JM, Meador-Woodruff JH. 2006. Expression of excitatory amino acid transporter interacting protein transcripts in the thalamus in schizophrenia. Synapse 59:394–402.

Inage YW, Itoh M, Wada K, Takashima S. 1998. Expression of two glutamate transporters, GLAST and EAAT4, in the human cerebellum: their correlation in development and neonatal hypoxic-ischemic damage. J Neuropathol Exp Neurol 57:554–562.

Itoh M, Watanabe Y, Watanabe M, Tanaka K, Wada K, Takashima S. 1997. Expression of a glutamate transporter subtype, EAAT4, in the developing human cerebellum. Brain Res 767:265–271.

Kalivas PW. 1993. Neurotransmitter regulation of dopamine neurons in the ventral tegmental area. Brain Res Rev 18:75–113.

Kanai Y, Hediger MA. 1992. Primary structure and functional characterization of a high-affinity glutamate transporter. Nature 360:467–471.

Kelland MD, Freeman AS, Rubin J, Chiodo LA. 1993. Ascending afferent

regulation of rat midbrain dopamine neurons. Brain Res Bull 31:539–546.

Kinoshita A, Shigemoto R, Ohishi H, Van der Putten H, Mizuno N. 1998. Immunohistochemical localization of metabotropic glutamate receptors, mGluR7a and mGluR7b, in the central nervous system of the adult rat and mouse: a light and electron microscopic study. J Comp Neurol 393:332–352.

Kita H, Kitai ST. 1987. Efferent projections of the subthalamic nucleus in the rat: light and electron microscopic analysis with the PHA-L method. J Comp Neurol 260:435–452.

Kita H, Kitai ST. 1988. Glutamate decarboxylase immunoreactive neurons in rat neostriatum: their morphological types and populations. Brain Res 447:346–352.

Kitai ST, Kita H. 1987. Anatomy and physiology of the subthalamic nucleus: a driving force of the basal ganglia. New York: Plenum Press.

Kugler P, Schmitt A. 1999. Glutamate transporter EAAC1 is expressed in neurons and glial cells in the rat nervous system. Glia 27:129–142.

Lehre KP, Danbolt NC. 1998. The number of glutamate transporter subtype molecules at glutamatergic synapses: chemical and stereological quantification in young adult rat brain. J Neurosci 18:8751–8757.

Lehre KP, Levy LM, Ottersen OP, Storm-Mathisen J, Danbolt NC. 1995. Differential expression of two glial glutamate transporters in the rat brain: quantitative and immunocytochemical observations. J Neurosci 15:1835–1853.

Liang J, Takeuchi H, Doi Y, Kawanokuchi J, Sonobe Y, Jin S, Yawata I, Li H, Yasuoka S, Mizuno T, Suzumura A. 2008. Excitatory amino acid transporter expression by astrocytes is neuroprotective against microglial excitotoxicity. Brain Res 1210:11–19.

Lin CL, Tzingounis AV, Jin L, Furuta A, Kavanaugh MD, Rothstein JD. 1998. Molecular cloning and expression of the rat EAAT4 glutamate transporter subtype. Brain Res Mol Brain Res 63:174–179.

London ED, Waller SB, Wamsley JK. 1985. Autoradiographic localization of [^{3}H]nicotine binding sites in the rat brain. Neurosci Lett 53:179–184.

Massie A, Cnops L, Jacobs S, Van Damme K, Vandenbussche E, Eysel UT, Vandesande F, Arckens L. 2003. Glutamate levels and transport in cat (*Felis catus*) area 17 during cortical reorganization following binocular retinal lesions. J Neurochem 84:1387–1397.

Massie A, Vandesande F, Arckens L. 2001. Expression of the high-affinity glutamate transporter EAAT4 in mammalian cerebral cortex. Neuroreport 12:393–397.

McCullumsmith RE, Meador-Woodruff JH. 2002. Striatal excitatory amino acid transporter transcript expression in schizophrenia, bipolar disorder, and major depressive disorder. Neuropsychopharmacology 26:368–375.

McGehee D, Heath M, Gelber S, Devay P, Role LW. 1995. Nicotine enhancement of fast excitatory synaptic transmission in CNS by presynaptic receptors. Science 269:1692–1697.

Mennerick S, Dhond RP, Benz A, Xu W, Rothstein JD, Danbolt NC, Isenberg KE, Zorumski CF. 1998. Neuronal expression of the glutamate transporter GLT-1 in hippocampal microcultures. J Neurosci 18:4490–4499.

Monaghan DT, Bridges RJ, Cotman CW. 1989. The excitatory amino acid receptors: their classes, pharmacology, and distinct properties in the function of the central nervous system. Annu Rev Pharmacol Toxicol 29:365–402.

Nagao S, Kwak S, Kanazawa I. 1997. EAAT4, a glutamate transporter with properties of a chloride channel, is predominantly localized in Purkinje cell dendrites, and forms parasagittal compartments in rat cerebellum. Neuroscience 78:929–933.

Nakanishi H, Kita H, Kitai ST. 1987. Intracellular study of rat substantia nigra pars reticulata neurons in an in vitro slice preparation: electrical membrane properties and response characteristics to subthalamic stimulation. Brain Res 437:45–55.

Otis TS, Brasnjo G, Dzubay JA, Pratap M. 2004. Interactions between glutamate transporters and metabotropic glutamate receptors at excitatory synapses in the cerebellar cortex. Neurochem Int 45:537–544.

Ottersen OP, Storm-Mathisen J. 1984. Neurons containing or accumulating transmitter amino acids. In: Björklund A, Hökfelt T, Kuhar MJ, editors. Handbook of chemical neuroanatomy. Vol. 3. Classical transmitters and transmitter receptors in the CNS. Part II. New York: Elsevier Science Publishers. p 141–216.

Parent A. 1986. Comparative neurobiology of the basal ganglia. New York: John Wiley & Sons.

Perry DC, Kellar KJ. 1995. [^{3}H]Epibatidine labels nicotinic receptors in rat brain: an autoradiographic study. J Pharmacol Exp Ther 275:1030–1034.

Petralia RS, Wenthold RJ. 1992. Light and electron immunocytochemical localization of AMPA-selective glutamate receptors in the rat brain. J Comp Neurol 318:329–354.

Pignataro L, Sitaramayya A, Finnemann SC, Sarthy VP. 2005. Nonsynaptic localization of the excitatory amino acid transporter 4 in photoreceptors. Mol Cell Neurosci 28:440–51.

Pinna G, Danbolt NC, Bjoras M, Zhang Y, Bendahan A, Eide L, Koepsell H, Storm-Mathisen J, Seeberg E, Kanner BI. 1992. Cloning and expression of a rat brain L-glutamate transporter. Nature 360:464–467.

Qu Y, Moons L, Vandesande F. 1997. Determination of serotonin, catecholamines and their metabolites by direct injection of supernatants from chicken brain tissue homogenate using liquid chromatography with electrochemical detection. J Chromatogr B 704:351–358.

Raiteri L, Raiteri M, Bonanno G. 2002. Coexistence and function of different neurotransmitter transporters in the plasma membrane of CNS neurons. Prog Neurobiol 68:287–309.

Rakhade SN, Loeb JA. 2008. Focal reduction of neuronal glutamate transporters in human neocortical epilepsy. Epilepsia 49:226–236.

Rauen T, Kanner BI. 1994. Localization of the glutamate transporter GLT-1 in rat and macaque monkey retinae. Neurosci Lett 169:137–140.

Ribak CE, Vaughn JE, Roberts E. 1979. The GABA neurons and their axon terminals in rat corpus striatum as demonstrated by GAD immunocytochemistry. J Comp Neurol 187:261–284.

Richardson KD, Jarret L, Finke EH. 1960. Embedding in epoxy resins for ultrathin sectioning in electron microscopy. Stain Technol 35:313–323.

Robertson SJ, Burnashev N, Edwards FA. 1999. Ca^{2+} permeability and kinetics of glutamate receptors in rat medial habenula neurones: implications for purinergic transmission in this nucleus. J Physiol 518:539–549.

Rothstein JD, Martin L, Levey AI, Dykes-Hoberg M, Jin L, Wu D, Nash N, Kuncl RW. 1994. Localization of neuronal and glial glutamate transporters. Neuron 13:713–725.

Rothstein JD, Dykes-Hoberg M, Pardo CA, Bristol LA, Jin L, Kuncl RW, Kanai Y, Hediger MA, Wang Y, Schielke JP, Welty DF. 1996. Knockout of glutamate transports reveals a major role for astroglial transport in excitotoxicity and clearance of glutamate. Neuron 16:675–686.

Saier MH. 1999. Eukaryotic transmembrane solute transport systems. Int Rev Cytol 190:61–136.

Sarre S, Yuan H, Jonkers N, Van Hemelrijck A, Ebinger G, Michotte Y. 2004. In vivo characterization of somatodendritic dopamine release in the substantia nigra of 6-hydroxydopamine-lesioned rats. J Neurochem 90:29–39.

Schmitt A, Asan E, Püschel B, Jöns T, Kugler P. 1996. Expression of the glutamate transporter GLT-1 in neural cells of the rat central nervous system: non-radioactive in situ hybridization and comparative immunocytochemistry. Neuroscience 71:989–1004.

Seal RP, Amara SG.1999. Excitatory amino acid transporters: a family in flux. Annu Rev Pharmacol Toxicol 39:431–456.

Sesack SR, Pickel VM. 1992. Prefrontal cortical efferents in the rat synapse on unlabeled neuronal targets of catecholamine terminals in the nucleus accumbens septi and on dopamine neurons in the ventral tegmental area. J Comp Neurol 320:145–160.

Shu S, Ju G, Fan L. 1988. The glucose oxidase-DAB-nickel method in peroxidase histochemistry of the nervous system. Neurosci Lett 85:169–171.

Slotboom DJ, Konings WN, Lolkema JS. 1999. Structural features of the glutamate transporter family. Microbiol Mol Biol Rev 63:293–307.

Sonders MS, Amara SG. 1996. Channels in transporters. Curr Opin Neurobiol 6:294–302.

Soriano E, Frotscher M. 1994. Mossy cells of the rat fascia dentate are glutamate-immunoreactive. Hippocampus 4:65–69.

Sotra KE, Harris KM. 1993. Occurrence and three-dimensional structure of multiple synapses between individual radiatum axons and their target pyramidal cells in hippocampal area CA1. J Neurosci 13:3736–3748.

Storck T, Schulte S, Hofmann K, Stoffel W. 1992. Structure, expression, and functional analysis of a Na$^+$-dependent glutamate/aspartate transporter from rat brain. Proc Natl Acad Sci U S A 89:10955–10959.

Takayasu Y, Iino M, Kakegawa W, Maeno H, Watase K, Wada K, Yanagihara D, Miyazaki T, Komine O, Watanabe M, Tanaka K, Ozawa S. 2005. Differential roles of glial and neuronal glutamate transporters in Purkinje cell synapses. J Neurosci 25:8788–8793.